UC San Diego
UC San Diego Electronic Theses and Dissertations

Title
Gene-Chip Diagnostics for Personalized Global Medicine

Permalink
https://escholarship.org/uc/item/61h3802c

Author
Hwang, Michael Taeyoung

Publication Date
2017

Peer reviewed|Thesis/dissertation

UNIVERSITY OF CALIFORNIA, SAN DIEGO

Gene-Chip Diagnostics for Personalized Global Medicine

A dissertation submitted in partial satisfaction of the

requirements for the degree Doctor of Philosophy

in

Materials Science and Engineering

by

Michael Taeyoung Hwang

Committee in charge:

Professor Ratnesh Lal, Chair
Professor Renkun Chen
Professor Guennadi Glinskii
Professor Xiaohua Huang
Professor Yuhwa Lo
Professor Donald Sirbuly

2017

The Dissertation of Michael Taeyoung Hwang is approved, and it is acceptable in quality and form for publication on microfilm and electronically:

_____

_____

_____

_____

_____

Chair

University of California, San Diego

2017

DEDICATION

For my wife, Sooyoung

EPIGRAPH

Now we are all sons of bitches.

Kenneth T. Bainbridge

TABLE OF CONTENTS

LIST OF FIGURES

LIST OF TABLES

ACKNOWLEDGEMENTS

2005   B. S. in Materials Science and Engineering, Seoul National University

2007   M. S. in Materials Science and Engineering, Seoul National University

2017   Ph. D. in Materials Science and Engineering, University of California, San Diego

PUBLICATIONS

Hwang MT, Shiah ZC, Antonschmidt L, Joon Lee, Glinsky G, Lal R, Wireless communication of label-free SNP detection using 2-D electronics and DNA nano-tweezers. Submitted

Hwang MT, Landon PB, Lee J, Choi D, Mo AH, Glinsky G, Lal R, Highly Specific SNP Detection Using 2D Graphene Electronics and DNA Strand Displacement. *Proc. Natl. Acad. Sci.* 2016

Mo AH, Zhang C, Landon PB, Janetanakit W, Hwang MT, Santacruz Gomez K, Colburn DA, Dossou SM, Lu T, Cao YB, Sant V. Sud P, Akkiraju S, Shubayev V, Glinsky G, and Lal R. Dual-functionalized Theranostic Nanocarriers. *ACS Applied Materials & Interfaces*. 2016

Hwang MT, Landon PB, Lee J, Mo A, Meckes B, Glinsky G, Lal R. DNA nano-carrier for repeatable capture and release of biomolecules. *Nanoscale.* 2015

Landon PB, Lee J, Hwang MT, Mo AH, Zhang C, Neuberger A, Meckes B, Gutierrez JJ, Glinsky G, Lal R, Energetically biased DNA motor containing a thermodynamically stable partial strand displacement state" *Langmuir*. 2014.

ABSTRACT OF THE DISSERTATION

Gene-Chip Diagnostics for Personalized Global Medicine

by

Michael Taeyoung Hwang

Doctor of Philosophy in Materials Science and Engineering

University of California, San Diego, 2017

Professor Ratnesh Lal, Chair

Single nucleotide polymorphisms (SNP) in a gene sequence are markers for variety of human diseases. Their detection with high specificity and sensitivity is essential for effective practical implementation of personalized medicine. Current DNA sequencing, including SNP detection, primarily uses enzyme based methods or fluorophore-labeled assays that are time consuming, need lab-scale settings, and are expensive. Electrical detection of DNA has been advancing rapidly, to achieve high

specificity, sensitivity and portability. However, existing electrical charge-based SNP detectors have insufficient specificity and accuracy limiting their effectiveness. Its actual implementation is still in infancy because of the low specificity, especially for analytically optimal and practically useful length of target DNA strands. Most of the research so far has focused on the enhancement of the sensitivity of DNA biosensors while the specificity problem has remained unresolved. The low specificity is primarily due to the non-specific binding during hybridization of probe and the target DNA. Here, we have addressed these limitations by designing a functional prototype of electrical biosensors for SNP detection. We demonstrate the use of DNA strand displacement-based probes on a graphene field effect transistor (FET) for single nucleotide mismatch detection. The single mismatch was detected by measuring strand displacement-induced resistance change and Dirac point shift in a graphene FET. SNP detection in large double helix DNA strands (e.g., 47 nucleotides) minimize false positive. We describe the first integrated dynamic DNA nanotechnology and 2-D material electronics, to overcome current limitations for the detection of DNA single nucleotide polymorphism (SNP). Existing SNP detection systems have poor specificity and lack portability and real-time wireless transmission of detected molecular signals. We have integrated two different kinds of dynamic DNA nano-devices as nucleic acid-sensing probes with electrical biosensors using graphene FET and analytical wireless communication platform. The signal was transmitted remotely using a microcontroller board and Bluetooth standard to personal electronics. Our electrical sensor-based SNP detection technology without labeling and without apparent cross-hybridization artifacts would allow fast, sensitive and portable SNP detection with single-nucleotide resolution. Practical implementation of this

enabling technology will provide cheaper, faster and portable point-of-care molecular diagnostic devices for personalized global health management.

Chapter 1.

Introduction to

cancer related gene detection

DNA sequencing has been of great interest for diagnosis of genetic disease[1], biological informatics[2], forensics[3], and environmental monitoring[4]. Discrimination of a single mismatch in a long DNA strand is of significant importance because it enables detection of single nucleotide polymorphism (SNP). An SNP is a single nucleotide mutation in a functional DNA sequence that varies among members of a biological species or paired chromosomes. These mutations are markers for variety of diseases, including various forms of cancer, genetic disorders[5], and can serve as biomarkers for personalized medicine[6]. Thus the development of biosensors with high sensitivity and specificity is especially important. DNA sequence detection methods, including SNP detection, are often enzyme-based methods and use DNA ligase[7], DNA polymerase[7] and nucleases[8]. These methods are utilized to generate highly accurate genotyping. However; they are generally expensive and time consuming. One of the dominant enzyme-free methods to detect SNPs employs hybridization of the target DNA to a probe on a microarray and detecting their binding events with fluorescence. DNA microarray for gene expression investigation is a high-throughput method and faster technique compared to PCR based

methods[9]. DNA microarrays use different DNA probes about 20-80 nucleotides (nt) in length in arrays to map >100,000 of DNA fragments in parallel. A target sample is tagged with a fluorescence label, and then reacted with probes on the chip. Only complementary sequence to probe is usually hybridized and detected based on fluorescent labeling (Figure 1.1). Hybridization-based methods for SNP detection have several disadvantages, including cross-hybridization between allele-specific probes[10]. This prevents high fidelity detection of a single mismatch in longer probe-target strand hybridization as the longer probes have more frequent cross hybridization. For example, a single mismatch in the center of 15 base pairs (bps) of probe-target duplex can be detected because there is critical difference in hybridization affinity between a perfect-matched and a single-mismatched hybridization. However, when the probe length is 40 or 50 nucleotides (nt), a single mismatch produces a relatively small difference between a perfect-match and a single-mismatched hybridization. Thus its detection is difficult with the simple hybridization-based methods. In general, the length of probes used in microarray is more than 20 nt, thus cross hybridization significantly reduces its reliability and specificity.

To reduce cross-hybridization, redundancies in the array design are used to verify detections of the same SNP or, probe sequences are modified to control the hybridization affinity[11]. For low cross-hybridization, fewer longer probes (60-80 nt) can attain similar reliable and sensitive detection[12]. DNA strand displacement can be used to improve specificity even for a longer probe. Strand displacement occurs when a DNA double helix exchanges one strand for another complementary strand[13]. The introduced strand holds higher affinity to one strand in the initial double helix and displaces another strand. Additionally, inosine or RNA can be used to control hybridization kinetics or Gibbs free

energy[14]. Strand displacement has been a core technique in DNA nano-manipulation for over 20 years and used in various mechanical nano-machines[15], logic gates[16] and sensors[14a, 17]. Currently strand displacement-based assays can discriminate SNPs efficiently by controlling competition between initially hybridized part in the double stranded or hairpin structured probe and probe-to-target hybridization[11a] (Figure 1.2).

The abovementioned methods have fluorescence-based readout. However, fluorescence-based sensors have limited life-time and background issues. Fluorescence-based detection also requires fluorimeters or laser scanners to analyze the optical signal. The field effect transistor (FET), a commonly used component in modern electronics, is of particular interest because it can be used as highly sensitive bio-molecular sensor and potentially can be integrated with hybridization measurement systems on a chip. Electrical detection of DNA using the field effect transistor (FET) has increased the detection sensitivity to femto-molar level[18]. Starting with silicon-based FET[19], recent interest has switched to 1-D materials such as carbon nanotubes[20] or Si nanowires[21]- due to their high surface-area-to-volume ratio and the sensitive carrier mobility to the electric field (charge density) they should provide better sensitivity. However tedious top-down fabrication process and random array of the materials adds to the high cost and reliability problems. A 2-D graphene sheet that is easy to fabricate consistently and has ambipolar field-effect, high carrier-mobility, low intrinsic electrical noise, mechanical strength and flexibility makes it a promising material for FET bio-sensing[22]. Graphene based bio-sensors have been developed to detect bacteria [23], glucose[24], protein[25], pH [26] and DNA[25, 27].

Microarrays for detecting SNP are readily available from Affymetrix, Illumina and other companies. The basic principle for SNP microarray is similar to the regular DNA microarray[28]. Variable probes with different mismatches to a normal gene are placed on microarrays. DNA samples are labeled with two different fluorescent dyes and treated with the probes on the microarray in the same amount. Fluorescence images are analyzed by quantifying the color with algorithms. The aforementioned non-specific hybridization can happen more frequently on SNP microarray than other kinds of DNA microarray as the 20-50mer probes only differ by 1 base pair (bp) between perfect matched (PM) and mismatched (MM) probes. This may results in a poor specificity and high background noise that can affect allele frequency estimates. SNP microarray utilizes very complex algorithms and redundant probes on different areas on the same microarray to avoid non-specific hybridization errors, wasting valuable time and materials[29].

To address these limitations, novel probes are needed that will eliminate cross-hybridization and detect SNP with high degree of specificity. In addition, a label free signal detection platform (without fluorescence reporter) that could be fabricated in a microarray format is preferred to achieve a high dynamic range.
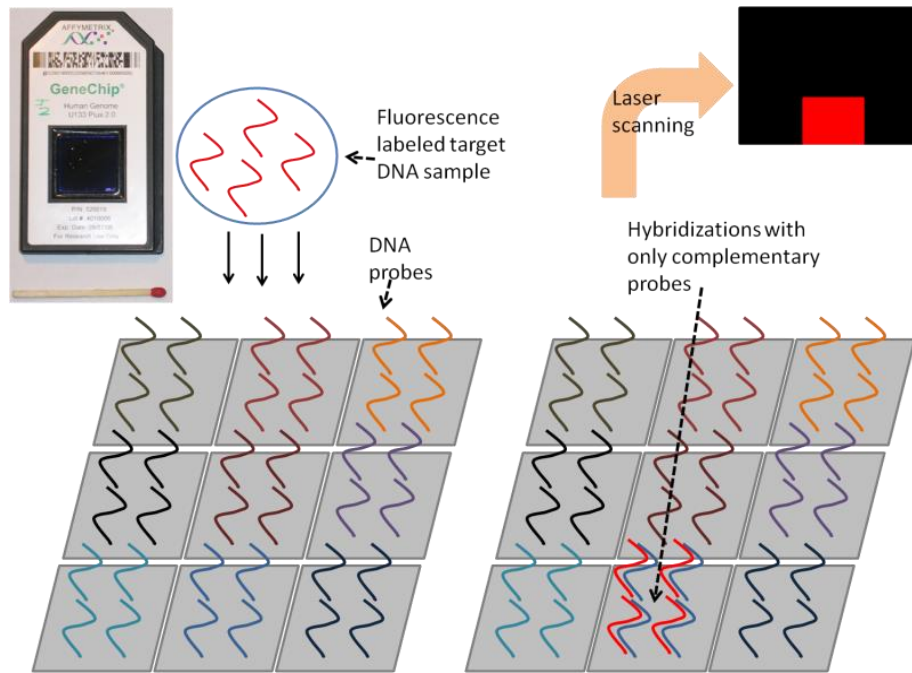
Figure 1.1. DNA microarray analysis; large number of spots are arrayed on a centimeter sized chip. Every spot has different DNA probes. When fluorescently labeled targets are put on the chip, it is hybridizes with its complementary probe and fluorescent. The chip is analyzed by laser scanner. (The microarray picture in left upper inset is from http://commons.wikimedia.org/wiki/File:Affymetrix-microarray.jpg)

Chapter 2.

Overall goal of the work

2.1. Developing an optimal probe for SNP detection

DNA nano-sensors such as the molecular beacon probe have been developed to increase specificity[11a, 30]. A molecular beacon probe is a stem-loop-folded hairpin structure of oligo-deoxyribonucleotide with fluorophore and quencher at each end of a strand (Figure 2.2a). A stem part is formed by partial complement over 5-10 bps among 25-30 nt of a single DNA strand. In the absence of a complementary strand to the molecular beacon probe, the fluorescence is quenched. When a complementary strand is introduced to the system, it breaks the hairpin of the molecular probe and fluoresces. However, single mismatched strand cannot efficiently separate the fluorophore and the quencher thus the fluorescence signal is much weaker than one with a complementary strand. 5-10 bps of the hairpin acts as a filter for a single mismatch. The Gibbs free energy of a hairpin is positioned between the energy of associated state for a mismatched and a perfect matched hybridization[31]. One mismatch among the target or probe reduces the affinity between the molecular beacon probe and the target strand vs. the affinity of a hairpin, thus the target strand cannot break the hairpin. Molecular beacon probe improves the specificity dramatically. However it requires relatively high concentration (~μM) of specimen, because 5-10 bps of hairpin is not stable enough at room temperature at lower concentration[32]. Moreover, a loop part is exposed singly and hairpin can be melted in

some conditions and interference among singly exposed probes can cause further complications. Length of the loop is limited to about 30 bps because such a longer strand has too strong affinity even with a single mismatched strand to keep hairpin structure, thus specificity will be detrimentally compromised.

We have recently developed DNA nano-device called a DNA zipper. It provides the physical movement of DNA segments by alternating each other (Figure 2.2b)[33]. Specifically, a DNA zipper contains three components: (i) a normal strand (N) containing only natural DNA bases [adenine (A), guanine (G), cytosine (C) and thymine (T)], (ii) a weak strand (W) containing inosine (I) substituted for guanine (with less energy than natural bonding to N), and (iii) the opening strand (O), which is a naturally complementary to N (table 1). N or W can have a short length of toehold to facilitate the reaction. W and N are weakly bonded than N and O therefore introducing O allows the zipper to open. Using the DNA zipper as a probe enables distinguishing PM and MM strands by its operation[14d]. A Fluorophore is attached to W and quencher to N to monitor the fluorescence signal. Initially the fluorophore is quenched as they are close to each other, when the DNA zipper is open it is brightened. W can act as a filter for SNP which has similar principle of molecular beacon probe. When there is one mismatch on O, its operation is poor as mismatched O cannot evict W fully from N. The operation of the DNA zipper is driven by competition among N, W and O therefore if O with a single mismatch does not have enough affinity to forfeit N from W, opening operation would not happen. The degree and distribution of energy between N and W can be modified by changing the number and location of I. There is not a single exposed strand on the probe thus it rules out the interference problem inherent with a molecular beacon probe. Also

concentration can be dropped to less than a few nM as the hybridization of N and W are more stable than 5-10 bps of hairpin on molecular beacon probe. Controlling the energy distribution over DNA zipper part, longer probes can also be designed.

Based on our recent data, a SNP observed in prostate cancer patients is identified between MM and PM with distinct fluorescence intensities (figure 2.3). <u>In the Specific Aim 1, using fluorescence-based DNA strand displacement analysis tools, we will design and validate the analytical performance of double-stranded probes for detection of disease-associated SNP variants in human sequences of DNA and RNA molecules.</u> The number and location of inosines and the toeholds length will be optimized for the most effective discrimination of SNP with the longest probe as possible. Many different kinds of SNPs will be tested to attain high-throughput sequencing simultaneously. *Once completed, we will have a probe not only capable of detecting SNP accurately, but also sensitive to added negative charge which can be an alternative signal transducer to fluorescence based microarray. This will constitute the Specific Aim 2 of the proposal.*

2.2. Developing an electronics-based sensor without fluorescence labeling

Two categories of sensing platforms without using fluorophore have been developed. First, as hybridized double stranded DNA (dsDNA) is heavier than single stranded DNA (ssDNA), the difference between dsDNA and ssDNA can be detected physically, using surface plasmon resonance (SPR)[34], surface acoustic wave (SAW)[35] and quartz crystal microbalance (QCM)[36]. Unfortunately, integration of mass-shift-based

DNA sensors is unrealistic as scanning mechanics are necessary to these sensors that are challenging and expensive. Therefore these sensing platforms are generally used for monitoring the single strand DNA dynamics but not in an array-format. DNA has negative charge due to its sugar phosphate backbone. Thus ionic charge difference between an ssDNA and a dsDNA is one fold. The difference between ssDNA and dsDNA can be measured if a field effect sensor is sensitive enough to detect a small charge of DNA[19, 37]. Thus a system sensitive enough to detect a small charge of DNAs would allow the detection of DNA hybridization. Also field effect transistor-sensor could be readily integrated in a microarray without the need for an expensive laser scanner and analyzer and hence can achieve high throughput and fast processing capability.

Electronic detection platforms such as field-effect transistor sensors can be ideal, because it is label-free and readily compatible with other electronic devices. It has been tried to detect negative charge of DNA by field effect transistor such as semiconductor[19], Si nanowire[37a, 38], carbon nanotube[39] and graphene[40] (figure 2.4). As charge of DNA is tiny, very sensitive platform is required to detect tens of DNA bps. Graphene has high potential as a sensing material owing to its high surface to area ratio. Graphene provides large detection area, biocompatibility, and exceptional electronic properties such as ultra-high mobility and ambipolar field-effect. However, despite its superior properties, graphene transistor for SNP detection with reliable discrimination with realistic length of probe and target has not been reported. This is because specificity of single strand probes is not enough to generate a distinct signal. The nano-DNA device based probes such as DNA zipper can be used to solve this issue and it is discussed in the following chapters.
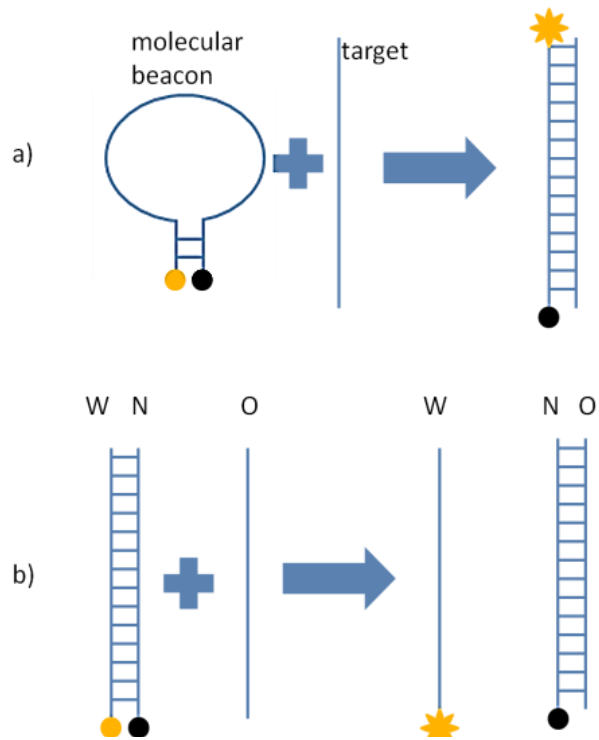
Figure 2.1. Operation of engineered probes; (a) when molecular beacon meets a target strand, hairpin structure is broken eliciting fluorescent signal (quencher is far from fluorophore). (b) When DNA zipper meets O strand, it separates zipper and hybridizes with N strand emitting fluorescent signal.
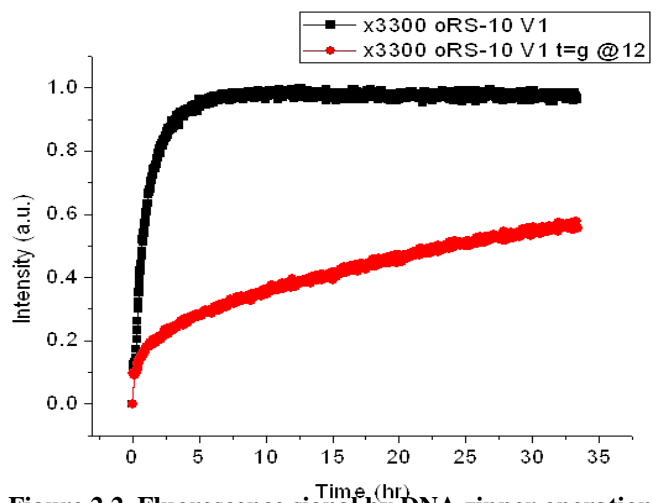
Figure 2.2. Fluorescence signal by DNA zipper operation; the black line shows rapid increase in fluorescence signal by opening of DNA zipper with perfect matched strand and the red line shows slow increase by poor opening of the DNA zipper with single mismatched strand of 25 base pairs.
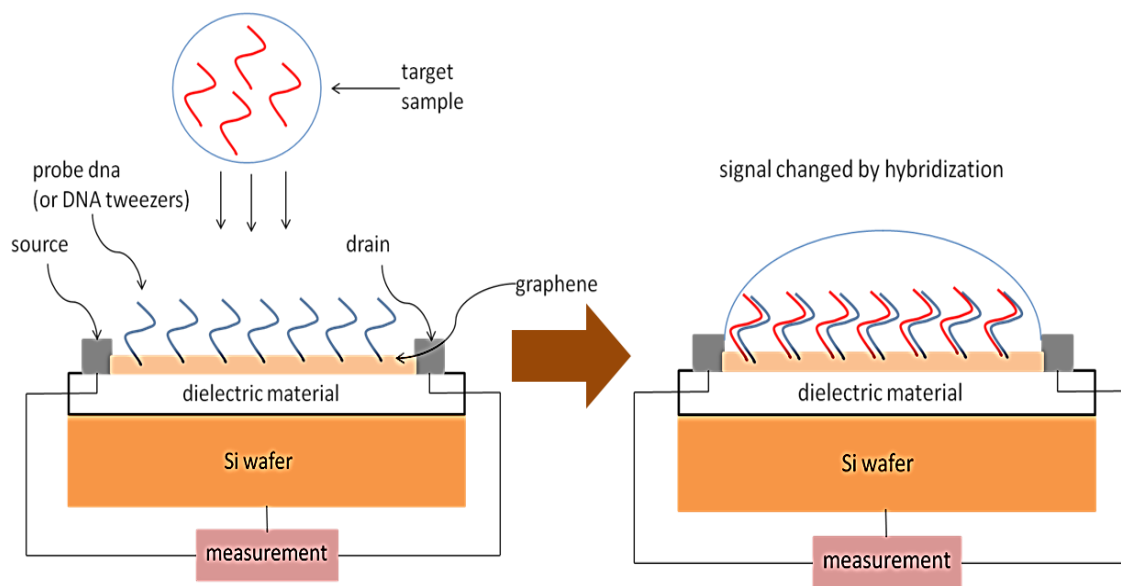
Figure 2.3. Schematics of electrical DNA sensing; probes are functionalized to sensing substrate, e.g., graphene. When targets are hybridized with probes, doubling of negative charge affects as negative doping on substrate.

Chapter 3.

Highly specific SNP detection using 2-D graphene electronics and DNA strand displacement

3.1. Abstract

Single nucleotide polymorphisms (SNP) in a gene sequence are markers for variety of human diseases. Their detection with high specificity and sensitivity is essential for effective practical implementation of personalized medicine. Current DNA sequencing, including SNP detection, primarily uses enzyme based methods or fluorophore-labeled assays that are time consuming, need lab-scale settings, and are expensive. Existing electrical charge-based SNP detectors have insufficient specificity and accuracy limiting their effectiveness. Here, we demonstrate the use of DNA strand displacement-based probe on a graphene field effect transistor (FET) for high specificity single nucleotide mismatch detection. The single mismatch was detected by measuring strand displacement-induced resistance (and hence current) change and Dirac point shift in a graphene FET. SNP detection in large double helix DNA strands (e.g., 47 nucleotides) minimize false positive. Our electrical sensor-based SNP detection technology without

labeling and without apparent cross-hybridization artifacts would allow fast, sensitive and portable SNP detection with single-nucleotide resolution. It will have wide applications in digital and implantable biosensors and high-throughput DNA genotyping with transformative implications for personalized medicine.

3.2. Introduction

DNA sequencing has opened new windows of opportunities for diagnosis of genetic disease [1], biological informatics [2], forensics [3], and environmental monitoring [4]. Discrimination of a single mismatch in a long DNA strand is of significant importance and is essential, in order to detect single nucleotide polymorphism (SNP). SNP is a single nucleotide mutation in a gene sequence and varies among paired chromosomes, between individuals, and across biological species. SNP mutations can have dramatic influence on the health, they are markers for variety of diseases, including various forms of cancer, genetic disorders [5], and are of critical importance for successful practical implementation of the concept of personalized medicine [6]. Thus, the development of biosensors detecting SNP mutations with high sensitivity and specificity is essential for effective personalized medicine undertakings.

Current DNA sequencing, including SNP detection is achieved primarily by enzyme-based methods, using DNA ligase [7], DNA polymerase [7] and nucleases [8]. These methods generate highly accurate genotyping. However; they are expensive and time consuming. One of the common enzyme-free methods to detect SNPs uses hybridization of the target DNA to a probe on a microarray and detects their binding events with

fluorescence microscopy/spectroscopy. Hybridization-based methods for SNP detection have several disadvantages, including cross-hybridization between allele-specific probes [10]. This limits the detection of a single mismatch in longer probe-target strand hybridization as the longer probes have more frequent cross hybridization. For example, a single mismatch in the center of 15 base pairs (bps) of a probe-target duplex can be detected because there is a critical difference in the hybridization affinity between a perfect-matched and a single-mismatched hybridization. However, when the probe length is 40 or 50 nucleotides (nt), a single mismatch produces a relatively small difference between a perfect-match and a single-mismatched hybridization. Thus its detection is difficult with the simple hybridization-based methods. The length of probes used in microarray is approximately 20 nt, thus cross hybridization significantly reduces its reliability and specificity. To reduce cross-hybridization, redundancies in the array design are utilized to confirm detections of the same SNP or probe sequences are modified to control hybridization affinity [11]. Utilization of longer probes significantly reduces or eliminates cross hybridization and fewer probes would be needed to obtain the same level of reliable analysis with longer probes (60-80 nt) [41] and they provide more sensitive detection [12].

DNA strand displacement can be used to improve specificity even for a longer probe design. Strand displacement occurs when a DNA double helix exchanges one strand for another complementary strand [13]. The introduced strand has higher affinity to one strand in the initial double helix and displaces the other strand. Additionally, inosine or RNA can be employed to control kinetics or Gibbs free energy of hybridization [14]. Strand displacement has been a core technique in DNA nano-manipulation for over 20

years and has been used in several mechanical nano-machines [15], logic gates [16] and sensors [14a, 17, 42]. Currently, strand displacement-based assays can discriminate SNPs efficiently, by controlling competition between initially hybridized part in the double stranded or hairpin structured probe and probe-to-target hybridization [11a, 42].

The broadly utilized SNP detection methods, even when the most advanced concepts of probe design being implemented, typically use the fluorescence-based readout. However, fluorescence-based sensors have life-time and background limitations. Moreover, they require fluorimeters or laser scanners to quantitatively analyze the optical signal and hence depend on a sophisticated and expensive lab-setting. Electrical detection of DNA sequences using the field effect transistor (FET) has recently been reported to lower the limit of detection to the femto-molar level [18]. FETs are of particular interest because they can be used as highly sensitive bio-molecular sensors and could be efficiently integrated using electric chip designs, including silicon-based FET [19],1-D carbon nanotubes [20], and Si nanowires [21]. Nanotubes and nanowires allow better sensitivity due to their high surface-area-to-volume ratio and the sensitive carrier mobility to the electric field (charge density). However tedious top-down fabrication processes and random array of the nanowires and nanotube resulted in high cost and reliability problems. Graphene, a 2-D material, is attractive because it is a single atom thick sheet that is easy to fabricate consistently over large areas. Ambipolar field-effect, high carrier-mobility, low intrinsic electrical noise, mechanical strength and flexibility collectively represent some of the advantages that make graphene a promising material for FET bio-sensing [22]. First generation graphene based bio-sensors have been developed to successfully detect bacteria [23], glucose [24], protein [25], pH [26] and DNA [25, 27].

FET-based DNA biosensors currently utilize a single stranded probe to detect hybridization. When the probe binds to the target strand a double helix forms and the binding results in a measureable change in the electric charge over the active layer of the FET [18, 43]. In currently available FET-DNA biosensors, the average length of the probe and the target is 10~25 nt [18, 20, 43-44]. In case of 25 nt probe, the signal difference between fully complementary target and single mismatched one is less than 50 % and it is significantly smaller than one reported with other biosensors utilizing short probes [20].

Given the inherent disadvantages of the current probe's design used in graphene FET biosensors, we reasoned that design, engineering, and fabrication of biosensors utilizing a strand displacement based probe architecture on a graphene FET would provide improved specificity and resolution. In this paper, DNA strand displacement based probe is successfully designed and utilized on a first-in-class graphene FET biosensor for label-free detection of a single mismatch with higher specificity than that of a single stranded probe DNA.

Architecture of double stranded (DS) probes was conceived to facilitate the design compatibility of a graphene FET biosensor for the electrical sensing of DNA strand displacement. A DS probe containing targeted inosine substitutions and optimized toehold lengths were first tested with fluorescence/quencher technology to demonstrate an efficient single mismatch discrimination. Then the non-fluorescently labeled DS probe was attached on a graphene FET to reproduce the SNP discrimination based on the electrical sensing of DNA strand displacement. The liquid gate was used to obtain I–V curve with DNA in buffer solution. I–V curve shifts and changes in resistance were

monitored with fully complementary (perfect match) and single mismatched DNA sequences. With this combination of the electrical sensor and dynamic DNA nanotechnology, a single mismatch was detected in 47 nt of DNA with high resolution. To our knowledge, this is the first report of the successful electrical detection of strand displacement in long DNA strands by sensing the charge difference before and after strand displacement without any labeling or additional processes.

3.3. Description of SNP Detection using Fluorescence Based Observations of Strand Displacement

The schematics of strand displacement and single mismatch detection are shown in Figure 3.1A. DS probe is prepared by hybridization of two complementary strands. The red strand in Figure 3.1 has a prolonged toehold section of 7 nt and its total length is 47 nt. The black strand is 40 nt and contains 4 inosine (I) substitutions, where guanines were originally located, to lessen the affinity between the two strands. The 47-nt side is called the normal side (N) and 40 nt side is called the weak side (W) as it contains I bases to weaken the double helix affinity. As shown in Figure 3.1, when 47 nt of target strand (T), which is fully complementary with the normal strand (N), is introduced to DS probe, it displaces the weak strand (W) and hybridize with the normal strand (N). Inosine (I) bases allow the shortening of the toehold part. If W does not contain inosines, hybridization affinity between W and N becomes too strong to efficiently displace W with T with the 7

nt of toehold; without inosine's substitutions, longer toehold is required to efficiently

displace W strand by T. Thus the strand displacement reaction can be summarized as the

following [45].
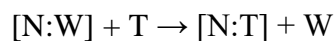
[N:W] + T → [N:T] + W

When T has a single mismatch to N, the affinity between N and T is significantly

decreased and the reaction rate is greatly reduced; DNA strands in the DS probe are not

displaced and it remains in its initial conformation (Figure 3.1, bottom) [14a, 14b].

The strand displacement was monitored over time with the fluorescence labeling

technique (Figure 3.2). A Texas Red fluorophore was labeled at the end of W and a

fluorescence quencher was labeled at the end of N. The quencher absorbed the emission

wave from the fluorescence when it was adjacent to fluorescence label, thus upon

hybridization of N and W, the fluorescence was quenched. When the perfect match T was

added on the sample, strand displacement happened,the fluorophore and quencher were

separated and the fluorescence signal became brighter. However, when the single

mismatch T strand was added, strand displacement happened at much slower rate and

much lower fluorescence signals were measured compared to a perfect match T

experiment. The length of the toehold affected the reaction rate and hence different length

of toeholds were tested. The test with 10 nt toehold showed vague discrimination of a

single mismatch because affinity between N and T was too strong with 10 nt toehold. The

two strands hybridized efficiently even with the single-mismatch.

In order to ascertain that the single mismatch T strand did not hybridize partially

from toehold part until the mismatched point, the discrimination was verified by DNA gel

electrophoresis. For DNA gel electrophoresis, the structure of DS probe was modified to accumulate T onto the DS probe, not just exchanging their position. Activity of the DS probe is not affected when W and N are bound by the hinge part when the hinge part was introduced to conform the DS probe partial-triple strand after strand displacement [45-46]. The details of the modification of DS probe are reported in the supplemental information. The gel image shows that the sample with the single mismatch T stained weaker than the sample with perfect match T, i.e, the single mismatch T did not displace W effectively compared to the perfect match T. Experimental protocols described above utilizing fluorescence-based detection of DNA strand displacement represent the standard experimental approach for the DS probe design optimization and fine-tuning of toehold lengths and inosine base substitutions for SNP detection using graphene FET biosensors.

3.4. Detection of Strand Displacement on Graphene FET

A graphene FET with two electrodes and a liquid gate chamber was fabricated to demonstrate electrical sensing of DNA using DNA strand displacement-based probes (Figure 3.1). The toehold part of N, which is adjacent to the graphene surface (Figure 3.1B, black dotted circle), became double-stranded after strand displacement and it changed the electrical signals as seen during the observations of the I-V curve and measurements of the electrical resistance. The graphene channel (4 mm $\times$ 6 mm) was transferred onto a silicon oxide-coated wafer using an established method [43, 47]. 1-Pyrenebutanoic acid succinimidyl ester (PASE) was used to link graphene and the amine

group at the N side of DS probe [18, 48]. The pyrene group of PASE and graphene were attached to each other by π-π stacking interactions to covalently link graphene/PASE to the amine group at the N side of DS prove.

The process of graphene functionalization was monitored at each step using an atomic force microscope (AFM). Graphene wrinkles ~4~7 nm in height are observed, these heights and shapes are in good agreement with the previosuly pubulshed results [23, 49]. PASE functionalization of graphene surface does not change the graphene surface roughness or morphology (Figure 3.3B). However, after immobilizing DNA on the graphene FET device through PASE and amine reaction, surface morphology was dramatically changed with the appearance of distinct globular structures (Figure 3.3C). The average height of these globular structures is 3.6 ± 1.4 nm and varies between 2 to 6 nm. The appearance of these structures seem consistent with the conformation of the standing DNA strands in fluid;. a typical height of double stranded DNA lying flat as detected by AFM imagiing in air is ~2 nm [50], which is significantly shorter than the height of globular structures in fluid observed in our experiments. DNA strands on the graphene FET device were further imaged in air after drying the graphene surface (Figure 3.3D). After drying, the appearance of dotted globular structures of double stranded DNA observed in fluid condition have changed to distinctive rod shapes of ~2 nm in height as shown in details of the inset image (Figure 3.3D). These observations were validated by the analyses of AFM images of graphene and PASE functionalized surfaces with and without DNA, which were also imaged in air. A DS probe consisted of a 40 bp double strand section and a 7 nt single strand overhang; in total the estimated length is ~15 nm. Consistently, the rod shapes of the DNA strands in the air AFM images show about

15~20 nm of length. Therefore, AFM images of devices in fluid and air conditins indicated that the PASE – amine functionalization strategy was working appropriately.

The conformation and position of the DS probe on the graphene surface is a critically important factor for the electrical detection of strand displacement. Only 7 nt of single stranded toehold of the 47 bps DNA becomes double stranded after the strand displacement compared to the initial DS prove (Figure 3.1). If the DS probe is lying down or absorbed on the surface, the signal difference would be too small to be detectable by recognizing the charge difference. The AFM image in Figure 3.3C shows that DS probe is observed as islands in liquid, while it was grain-boundary-shape in air (Figure 3.3D). When the surface was fully covered by PASE and ethanolamine, the DS probe was not exposed and not absorbed into graphene except amine-amide bonding, otherwise nucleotides can be absorbed to graphene by π-π stacking interaction. Additionally, molecular dynamics simulations have shown that DNA established an upright conformation to the silica surface, fluctuating only around 10° from vertical at stable state [51]. We thus concluded that the positioning of DS probes is perpendicular to the graphene surface in liquid and the functionalization strategy was successful.

The source and drain electrodes were applied by silver paste and silicone rubber were used before the DNA probe functionalization to insulate the electrodes and create solution reservoir [47]. Sample in buffer solution was placed in the reservoir and a gate voltage was applied directly to the top of the buffer solution [18, 22, 25, 43]. When the surface charge was changed by strand displacement, the charge built up and the I-V curve shifted to left side and the resistance was increased [18, 43, 47]. Functionalization of DS probe

changed electrical signals of FET. The I-V curve was measured after PASE is fixed on

the graphene channel with $1 \times$ PBS buffer solution as liquid gate. After DS probe was

bonded on the PASE, the measurement was repeated again. The I-V curve shifted to left

side after the bonding of DS probe. The resulting unique U-shaped I-V curve is due to the

ambipolar characteristic of graphene. Additionally the electrical resistance increased and

shifted the I-V curve lower.

The Debye length should be considered when detecting electrical charge in ionic

solultion [52]. It can be written for aqueous solution at room temperature as

$$\lambda \, (nm) = \frac{1}{\sqrt{4\pi I_B \sum_i z_i{}^2 \rho_i}}$$

where λ is the Debye length expressed in nanometer, I_B is Bjerrum length which is about

0.7 nm, z_i is valencies of the various types of ions and ρ_i is number densities or number

of molecules per volume [53]. Note that it is an estimate of the distance where Coulomb

interactions are ignored, so does the size of the region near a point charge where

opposite-charge counterions can be found. It represents the net length of the electrostatic

effect in ionic solution. Charges are electrically screened outside the sphere whose radius

is the Debye length. In the $1 \times$ PBS solution, which is generally used as a DNA buffer

solution, its Debye length is less than 1 nm. More diluted PBS such as 0.1 or $0.01 \times$ PBS

allows detection of the longer part of the hybridization. However, the DS probe requires a

high ionic concentration to stably operate the strand displacement. If the ionic

concentration of buffer solultion is too low, its double helix structure can be unstable and

could fail in strand displacement.

For measurning the effect of strand displacement, 12.5 mM $MgCl_2$ and 30 mM Tris buffer was used to increase Debye length. This $MgCl_2$ concentration is known to be equivalent to about $1 \times PBS$ for DNA helix stabilization [54]. $MgCl_2$ is 2:1 electrolyte (e.g. $Mg^{2+}:2Cl^-$) and its Debye length of 12.5 mM $MgCl_2$ is calculated by the above equation to be ~ 1.6 nm. The electrical effect of DNA is reproteted to be rapidly decreased and that only a few sequences which are close to the graphene surface determine the electrostatic potential on the sensor [55]. Thus the first few sequences would have effective charges on the surface. The tests were also conducted with $1 \times PBS$ and compared with $MgCl_2$ buffer solution. The $MgCl_2$ buffer solution generated clearer discrimination.

In order to examine the specificity of the graphene FET sensor, perfect match and single mismatch samples were tested. Target strands in different concentrations (100 nM to 100 μM) were incubated on the sensor for 8 hours (Figure 3.4). When the perfect match T was treated on the graphene sensor, the U-shaped I-V curve shifted down and to the left, which indicates increasing resistance and imposition of n-doping effect [18, 43]. The corresponding resistance change was observed as discussed below. With 100 nM of T strands, which is equivalent to about 3.011×10^{12} of T molecules in 50 μL of buffer solution, DS probe showed clear discrimination of single mismatch (Figure 3.4). As the concentration of the perfect match T was increased, I-V curve kept shifting and the shape of the curve became flattened. As shown in the Figure 3.4C, the Dirac-point of the I-V curve was shifted ~-50 mV with 100 μM of perfect match T and ~-11.6 mV with single mismatch T (4.3-fold difference). Defferent values of source voltages were also tested and it also showed the same trends of Dirac point shifts. Signifcantly, the single mismatch T made much smaller shifts and the I-V curve was saturated. It is reasonable to

believe that a single mismatch T could not result in the proper strand displacement while a perfect match T could induce a proper strand displacement. Our results show a clear discrimination of a single mismatch in the 47 bp DNA probe, suggesting that it could be possible to detect single mismatch in a longer DNA strand.

The resistance change of the channel was measured and compared between the perfect match and the single mismatch targets at different concentrations (Figure 3.4). When DNA is accumulated on the graphene surface, its resistance increased [44]. Immobilization of DS probe and addition of target strands increased the resistance of the channel. The resistance increased 40~60 % when the probe was anchored on the graphene surface. As shown in the Figure 3.4C, perfect match T increased the resistance significantly more than single mismatch T. The largest difference was observed at a target concentration of 100 nM with the resistance changes of ~26.0 % and ~6.8 % (3.8-fold difference) for the perfect match and the single mismatch T, respectively. The minimum difference was observed at the target concentration of 100 µM with the resistance changes of ~84.9 % and ~46.0 % (1.8-fold difference), for the perfect match and the single mismatch, respectively.

In control experiments, single strand probes were tested using only the N side of DS probe, to confirm that the discrimination of single mismatch in 47 bps resulted from using DS probe. The single mismatch target strands were tested with the concentration ranging from 10 pM to 1 nM. When a single mismatch target strand was hybridized with N side of the probe, its signal transferred as much as the DS probe with the perfect match target. The concentration of the T strand needed to saturate the I-V curve transfer was

much lower because it does not have the W side of DS probe. When it was a DS probe, T strand needed more energy (higher concentration) to displace the W strand. Single mismatch target strand shared identical 27 nt and 19 nt with the perfect match target and the melting temperature of hybridization of single mismatch target and N side is 55-65 °C with concentration range of 10 pM to 10 μM [56].

The stable hybridization of single mismatch target and the normal strand (N) made the discrimination of the single mismatch impossible when the probe was single stranded. These results indicate the superior capability of DS probe on graphene FET to discriminate a single mismatch in long DNA sequences.

Originally microarrays used photolithography to fabricate micro-sized spot arrays inspired by transistors array in electronics. The proposed graphene FET biosensor can also be integrated in the form of microarray. These array sensors would not need fluorescence labeling or optical components and would reduce the required number of spots for indivudual sequences by detecting strand displacement of longer DNA strands. It seems likely that specificity of the graphene FET sensor described in this work is suffiently high to alleviate the need for complex algorithms to analyze vague data for the detection of SNP as it is necessary with current technology. As such, the further development and imlementation oof this technology would allow more affordable and accurate diagnosis of a myriad of diseases, including cancer, degenerative, various and genetic disorders.

3.5. Conclusions

Label-free detection of a single mismatch in 47 bps probe with high resolution was achieved by using DNA strand displacement on a graphene FET chip. This was possible by electrical sensing of the inherent charge of DNA with the graphene transistor. Utilizing a double-stranded probe capable of detecting a single mismatch in 47 bp double helix, the perfomance of the sensors appears to exceed signifcantly the performance of a single-stranded probe. The strucutre of double stranded part in the probe was changed by strand displacement and this difference was readable in the electrostatic gating effect. The SNP-discrimination results are readily detectable in the I-V curve and resistance. Electrical detection of a single mismatch was also correlated with the real time fluorescence measurement. The work provides a significantly improved platform for SNP detection by combining high fidelity probe design and the detection scheme that has not been reported previously. Our results demonstrate the practical utility of the novel biosensor technology based on a combination of dynamic DNA nanotechnology and 2-D nanoelectronics. It opens opportunities for the development of more reliable and efficient diagnostic tools for early detection of potentially life threatening human diseases, including design and development of the miniaturized, point-of-care and implantable biosensors.

3.6. Methods

3.6.1. Materials

PASE, ethanolamine, $MgCl_2$ and conducting silver paste were obtained from Sigma Aldrich (Saint Louis, MO).Graphene from ACS material (Medford, MA). Silicone

rubber from Dow Corning (Midland, MI), PBS and Tris solution from Thermo Fisher Scientific (Waltham, MA), Poly (methyl methacrylate) (PMMA) from MicroChem (Westborough, MA), Ammonium persulfate from MP Biomedicals (Solon, OH), DNAs from IDT (Coralville, IA). DNA gels from Lonza (Walkersville, MD) were obtained, respectively. All the DNA sequences for this experiment appear in Table S1. Ultrapure water was from a Millipore purification system.

3.6.2. Fluorescence Test

Normal strand (N) side which was tagged with fluorescence quencher and the weaker strand (W) side with fluorescence label are mixed in ratio of 1:1 in $1 \times$ PBS solution and annealed from 20 ℃ to 90 ℃ and cooled it to 4 ℃ over 3 hours. A Texas Red has excitation maximum wavelength of 596 nm and emission maximum wavelength of 613 nm. Perfect match and single mismatch T strand are all suspended in $1 \times$ PBS. The hybridized DS probe was diluted in $1 \times$ PBS into 20 nM and tested using a Tecan Infinite 200 M plate reading spectrometer (San Jose, CA) at 27 ℃ with an accuracy we estimate to be approximately ± 1.5 °C. Excitation/Emission of TEXAS red are observed at 590/620 nm. Each experiment began with a 50 µL sample volume with a device concentration of 20 nM (20nm of DS probe and 100 nM of T) in black 96 well plates. Clear microplate sealing films were applied over the sample wells to avoid evaporation. The same test was conducted in $1 \times$ PBS buffer solution.

3.6.3. Fabrication of Graphene FET

The top side of graphene on a copper film was spin-coated with PMMA to protect the top side of graphene while the bottom side of graphene was etched away. PMMA acted as the supporting layer of the graphene after etching the copper. The back side of graphene was removed by oxygen plasma etching. The sample was cut into 4 mm × 6 mm pieces with scissors. Copper was etched by floating on 0.1 M of ammonium persulfate for about 5 hours and rinsed in DI water overnight. Graphene supported by PMMA was then transferred on SiO_2 coated silicon wafer. PMMA layer was removed by acetone at 60 °C for 1 hour. The sample was annealed at 300 °C for 2 hour under hydrogen/argon atmosphere [57]. To fabricate transistor, conducting silver paste was used as source and drain electrodes at the two ends of the graphene. Silicone rubber was used to insulate source and drain electrodes from liquid and construct solution reservoir.

3.6.4. Immobilization of DS Probe

5 mM of PASE in Dimethylformamide (DMF) was treated on the graphene for 1 hour and rinsed with pure DMF and DI water. 50 µM of DS probe was added on PASE-modified graphene for 2 hours. The graphene FET with DS probe functionalization was rinsed with 1 × PBS. 100 mM of Ethanolamine solution was treated to saturate the possibly unreacted amino group on PASE and rinsed with 1 × PBS solution. Volume of all treated chemicals and samples was 50µL.

3.6.5. Visualization of DNA and graphene surface

Topographic images of DNA on graphene surface were acquired using a Multimode atomic force microscope equipped with a Nanoscope V controller (Bruker). Silicon cantilevers with a spring constant of 42 N/m (PPP-NCHR, Nanosensor) were used for imaging in air using tapping mode. Silicon nitride cantilevers with spring constants of 0.08 N/m (OMCL-TR400, Olympus) were employed for imaging in fluid using peak force tapping mode. The Nanoscope software was used for analyzing imaging data.

3.6.6. Strand Displacement on the Chip

Strand displacement reaction was conducted by dropping perfect match and single mismatch T strands with concentrations which are indicated in the legends of data and incubated overnight in the reservoir on the graphene FET chip. Then the chip was rinsed gently with $1 \times$ PBS. All the volume of treated samples was 50µL.

3.6.7. Electrical Measurements

I – V curves and resistance were measured in a semiconductor parameter analyzer equipped with a probe station. Silver wire was used as electrode which applied Vg to the 12.5 mM $MgCl_2$ - 30 mM Tris buffer solution. Tests were also conducted with $1 \times$ PBS buffer solution. Gate voltage (Vg) was swept from -0.5 ~ 1 V and drain – source voltage (Vds) was picked between 0.05 ~ 0.3 V. Drain – source current (Ids) was measured at an assigned Vds. Resistances were measured at 50 mV of Vds.

Chapter 3 in part is a reprint of the material Hwang M. T., Landon PB, Lee J, Choi D, Mo AH, Glinsky G, Lal R. Highly specific SNP detection using 2-D graphene electronics and DNA strand displacement. *Proc. Natl. Acad. Sci.*. 2016; vol. 113 no. 26: 7088–7093. The dissertation author was the primary author.
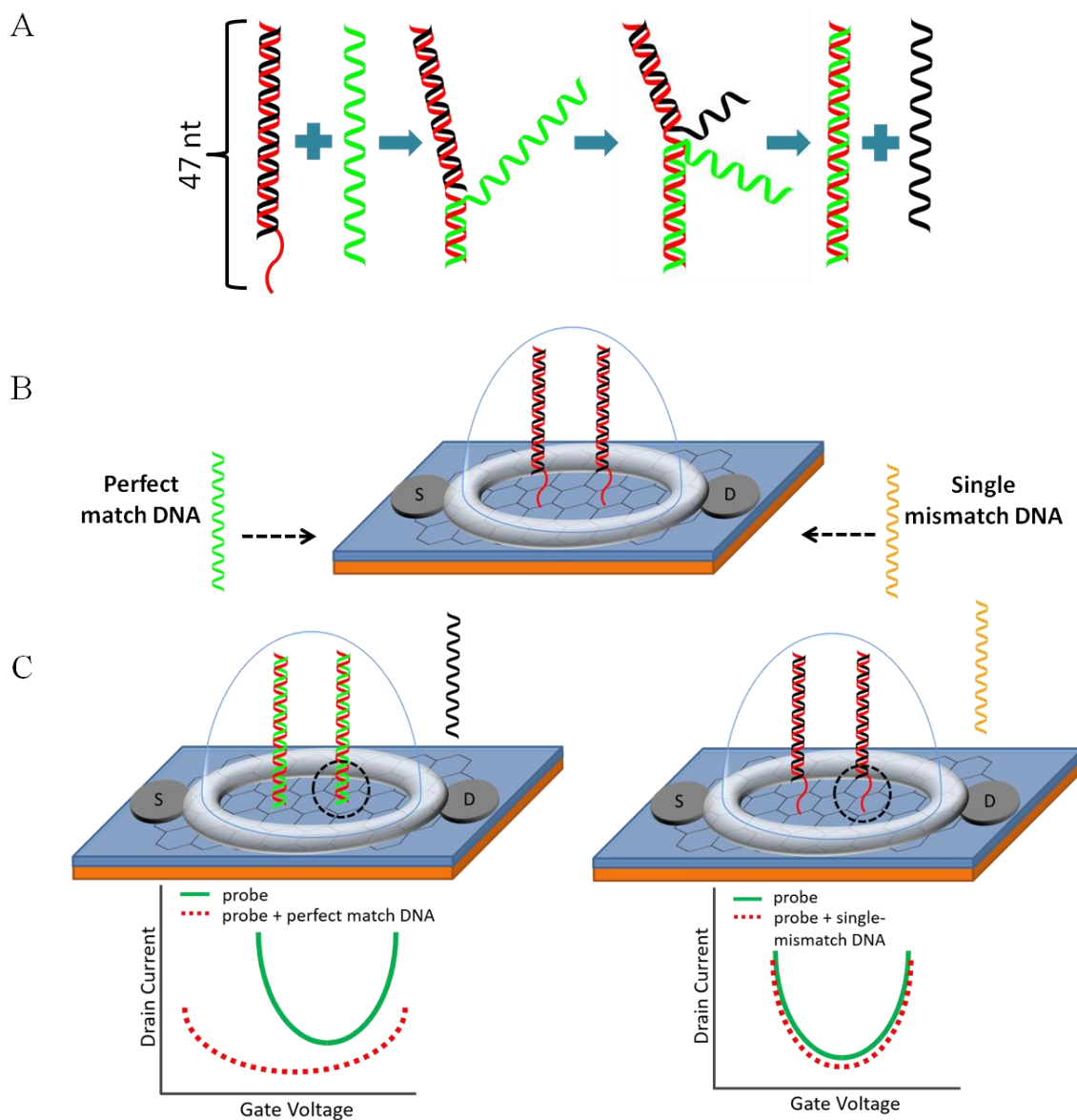
Figure 3.1. Schematics of the gene chip sensor. A) Double stranded probe (DS probe) action. The red strand is normal strand (N) and contains 7 nt of toehold. Toehold is single-stranded at the initial state. When a perfect match target strand (green strand) approaches a DS probe, it displaces the weak strand (black strand, W) by binding to the toehold. B) Graphene FET sensor with DS probe. 'S' and 'D' represent source and drain of FET. Gate voltage is applied directly on the liquid gate; the liquid gate is shown as a hemisphere (light blue) surrounding the DS probe. C) Left panel: The green strand displaces the black strand and the toehold portion becomes double-stranded (black dotted circle region). Right panel: A target strand with single mismatch (yellow strand) does not allow the strand displacement properly, i.e., the yellow strand does not displace the black strand. Thus the toehold region remains single-stranded (black dotted circle). D) Current-voltage relaionship (IV curve) due to charge difference during the strand-displacement in the gene chip FET sensor. Left panel: IV curve for strand displacment with perfect match (C, Left panel). The IV curve shifts leftside and downside. Right panel: Single mismatch target strand does not displace the black strand properly; thus the IV curve remains almost the same.

A

Target DNA

Perfect match: 5'-TGA AAG GGT TTT AAT AAT AGA ATT TTA AAA GAC TGG TAG AAA TAA GG-3'
Single mismatch: 5'-TGA AAG GGT TTT AAT AAT A*T*A ATT TTA AAA GAC TGG TAG A AA TAA GG-3'

B

N+W   T   N+T   W

C
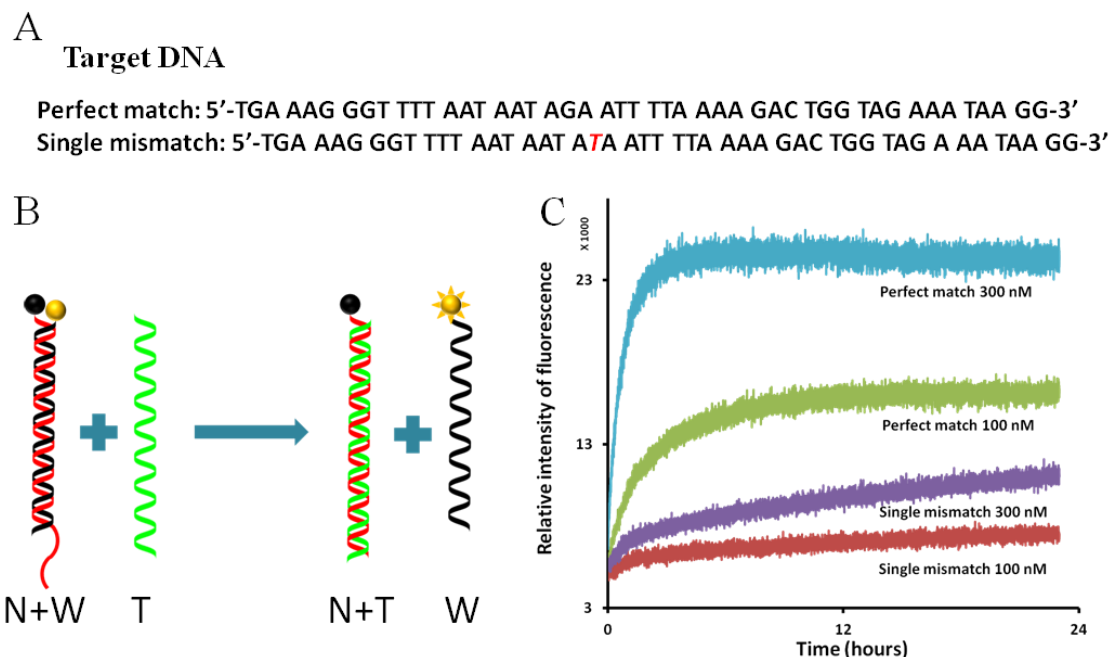
Figure 3.2. Single mismatch detection using fluorescently labeled nucleotides. A) Sequences of the target DNA. Top: perfect match. Bottom: single mismatch. The mismatched nt is marked in red color. B) Schematics of strand displacement: nt with fluorphores (yellow ball) and nt with quencher (black ball). Initially the normal (N, red) and weak (W, black) strands are hybridized, fluorophore (yellow ball) and quencher (black ball) are adjacent so that fluorescence is quenched. When green strand (perfect match T) interacts with DS probe, strand displacement takes place, normal strand (N) and perfect match target strand hybridize. Weak strand (W) remains single-stranded and fluorophore becomes active. B) Real time fluorescence measurement of the strand displacement. Interaction of the single mismatch target strand with DS probe shows much less fluorescence activity than the interaction of the perfect match with DS probe. The concentration of DS probe was 10 nM and the concentrations of Ts varied from 100 nM to 300 nM shown under each plot.
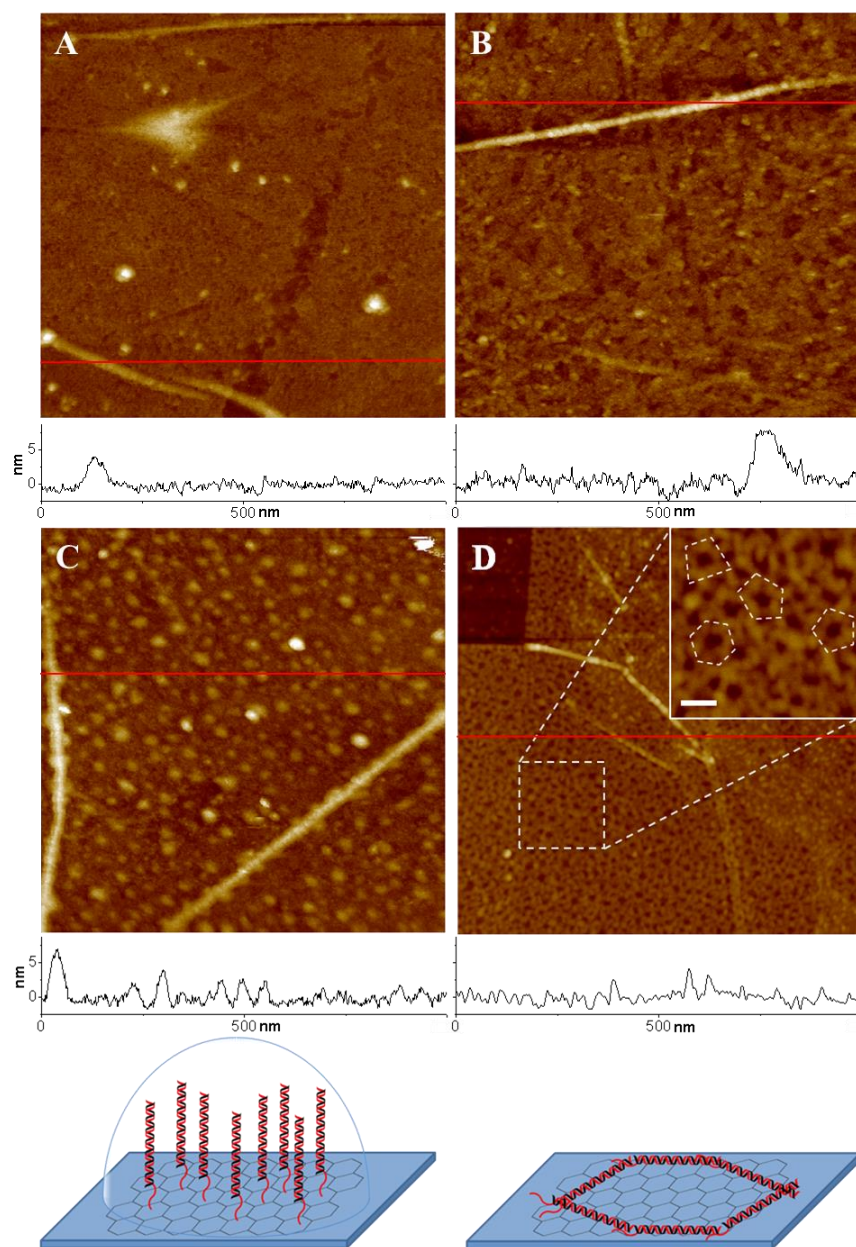
Figure 3.3. AFM images of graphene transistor surface with and without DNA strands. A) Graphene surface in fluid is mostly flat with some defects (black arrows) and graphene wrinkles (blue arrows). B) PASE coated graphene surface in fluid shows flat surface with similar wrinkle height of 7 nm. C) After binding of double strand DNA on the PASE coated graphene surface in fluid, graphene's smooth surface is covered with DNA strands ~ 2-4 nm in height. The graphene wrinkles height remains the same. D) DNA strands are visualized better in air AFM image with distinctive appearance of DNA structures. Inset image shows more details of DNA structures at higher magnification. The randomly lying DNA probes in the inset are outlined with dot line. Surface height profiles at the red line are plotted at the bottom of each image. Cartoons at the bottom represent models of formation of DNA structure in liquid and air. The right cartoon renders the random polygonal structure of DNA in air. All images have scan area of 1 x 1 μm and a z-range of 20 nm except for inset. The z range and the scale bar of the inset is 10 nm and 50 nm, respectively.

Target DNA

Perfect match T: 5'-TGA AAG GGT TTT AAT AAT AGA ATT TTA AAA GAC TGG TAG AAA TAA GG-3'
Single mismatch T: TGA AAG GGT TTT AAT AAT A*TA* ATT TTA AAA GAC TGG TAG A AA TAA GG-3'
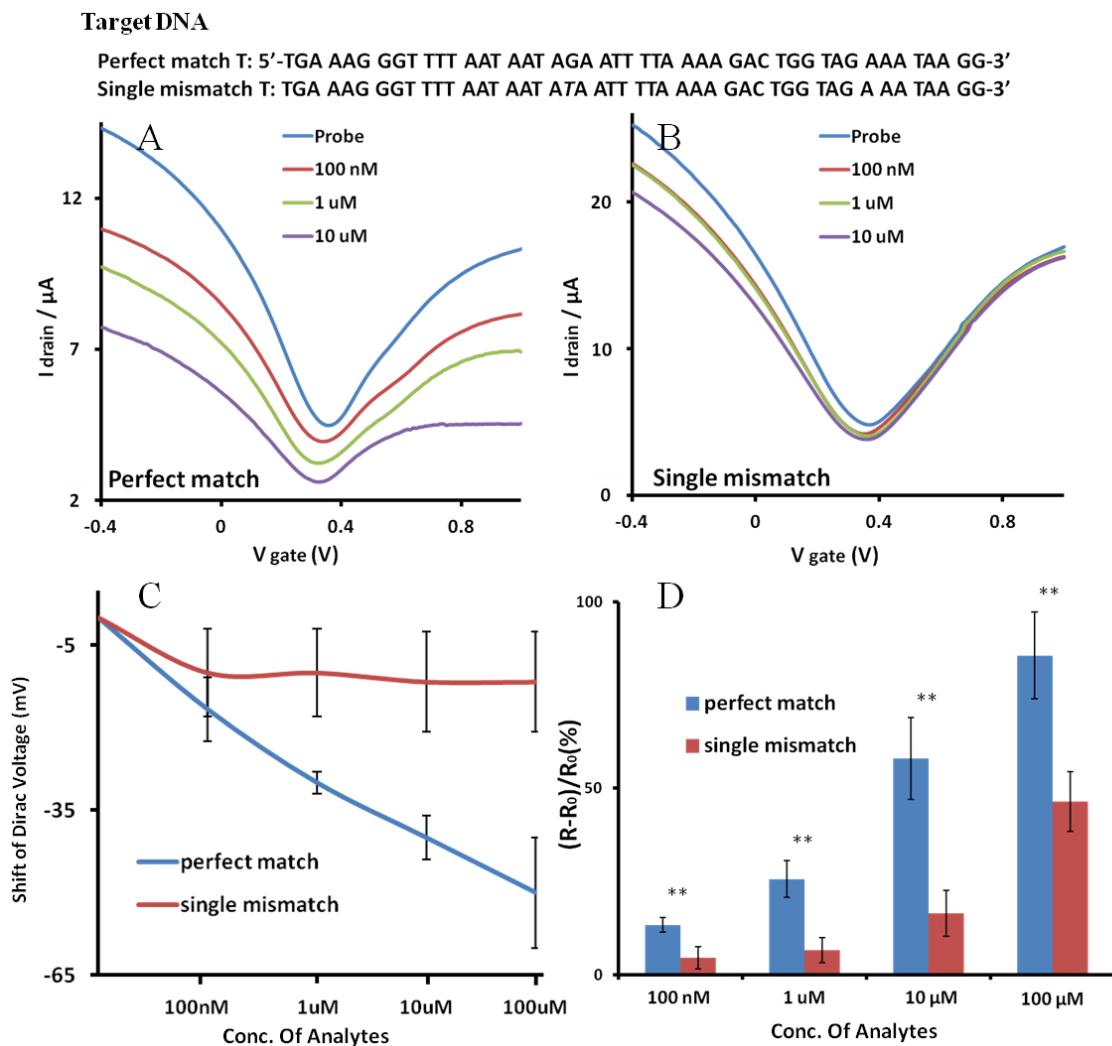
Figure 3.4. I-V relationship of the graphene FET sensor for the strand displacement reactions. A) The perfect match T shifted the IV curve according to concentrations B) The single mismatch T shifts the IV curve significantly less. The DNA sequences of T used in the experiments are shown over the IV curve. C) A statistical summary of Dirac voltage shift of the FET sensor shown in panels A and B. The Dirac voltage is expressed as a function of the concentration of the added target DNAs. D) Distinguishable resistance change of the channel layer caused by strand displacement at different concentrations of the T DNAs. Statistical values (mean +/- SD) were based on three sets of data points for each case. $n = 3$. **$P < 0.01$.

Chapter 4.

Wireless communication of label-free SNP detection using graphene field-effect transistor and strand displacement in DNA nano-tweezers

4.1. Abstract

Single nucleotide polymorphism (SNP) detection and DNA sequencing for identification of mutations are of great interest in personalized medicine, forensics and environmental monitoring. Existing SNP detection systems have poor sensitivity and specificity and lack portability and realtime wireless transmission of detected molecular signals. We have integrated DNA nano-tweezers, a dynamic DNA nano-device, as a nucleic acid-sensing probe with electrical biosensors using graphene FET and analytical wireless communication platform. SNP detection was achieved by observing changes in Dirac point shift in IV curve and resistance change due to the hybridization of a probe DNA and a target DNA strands. DNA nano-tweezers probe significantly improved analytical

characteristics of SNP detection. The electrical signal resulting from resistance changes triggered by DNA strand-displacement in the DNA tweezers was recorded. The signal was transmitted remotely using a microcontroller board and Bluetooth standard to personal electronics, including smart phones, tablets and computers. Practical implementation of this enabling technology will provide cheaper, faster and portable point-of-care molecular diagnostic devices for personalized global health management.

4.2. Introduction

The detection and sequencing of DNA and RNA molecules for diagnostics,[1] forensics[3] and environmental monitoring[4] is of great interest in personalized precision medicine. Current DNA detection methods primarily use fluorescent labeling and require laboratory scale settings such as fluorimeters or laser scanners to analyze optical signals. Miniaturized chip-based electrical detection of DNA will eliminate the aforementioned limitations enabling in-field or at home detection of specific DNA sequences.[58] Electrical sensing-based methods have successfully lowered the limit of sequence specific DNA detection to the femto molar level.[21, 48, 59] A field effect transistor (FET) can be employed as a highly sensitive DNA sensor and can potentially be integrated with other on-chip analytical systems.

Graphene is an attractive electronic material of choice for a biosensing platform because it has high sensitivity to the changes in carrier mobility with respect to changes in the gating electric field, low intrinsic electrical noise, mechanical strength and flexibility.[22, 60] We recently have reported DNA strand displacement based-probe on graphene FET for

SNP detection in relatively long nucleic acid sequences with unprecedented specificity. SNPs are markers for a variety of diseases, including various forms of cancer, genetic disorders, and are of critical importance for successful practical implementation of the concept of personalized medicine.[61] Thus, detection of SNP mutations with high specificity and sensitivity is essential for a broad range of diagnostic applications and effective implementations of personalized precision medicine approaches.[11b, 11c, 17, 62] With the proof-of-concept experiments demonstrating in principle the feasibility of the approach successfully addressed, a more complex design of the probe mechanism could be useful to achieve better functionalities and facilitate nano-scale engineering of electrical biosensors. Another advantage of using an electrical signal-based DNA sensor is its compact size and portability compared to current fluorescence-based techniques. Also, a fully integrated electronic sensor and signal measurement system can transmit signals using wireless systems on a portable computing device such as a smart phone. Graphene-based wireless detection of macro-sized bacteria has been reported.[63] However, highly specific detection of biomolecules with relatively small electrical charges, such as DNA or RNA molecules, has not been demonstrated until very recently.[60b] Electrical signal-based DNA sensors will facilitate unsophisticated end-users access to DNA detection chip technology.[64]

In this manuscript, we report a DNA nano-device comprising of DNA nano-tweezer-based nucleic acid-sensing probes engineered to achieve the improved analytical performance of electrical biosensors which is documented by better specificity and higher signal to reference ratio.[60b] We also demonstrate the practical implementation of a wireless electrical signal-based DNA sensor using a graphene FET chip. First, design of

DNA nano-tweezer-based probes was tested and optimized for detection of SNP with fluorescently-labelled DNA nano-tweezers. Then DNA nano-tweezers without the fluorescent label were immobilized onto the graphene surface by π-π stacking and amine-amide bonding as previously reported.[60b, 65] The patterns and efficiency of immobilization of DNA nano-tweezers were verified with atomic force microscopy (AFM) imaging. The detection of SNP was then carried-out with the graphene FET sensor. The analytical performance of the graphene FET biosensor was examined by the electrical signal-based detection of the DNA strand displacement with target DNA that drove the strand displacement and opening of the DNA nano-tweezers on the chip. When the DNA nano-tweezers open, it causes the switching of varied lengths of strands and this in turns causes a charge difference before and after strand displacement without any labeling or additional processes. This results in the changes in the measured resistance and Dirac-point of the graphene (Fig. 1 and 6).

To implement wireless capabilities, the graphene DNA chip was connected to a proprietary wireless system using a microcontroller board. A flow chart of the top-level design of graphene chips communication with the smartphone is presented in Fig. 2 with different operation aspects highlighted by a color code (Blue: Communication, Red: Signal Generation, Black: Measurement). The details of low-level design are presented in Fig. S1. The microcontroller board was a Freescale FRDM-KL25Z with serial support, I2C and UART communication protocols. It also provides Pulse-Width-Modulation (PWM) signal output and Analog-to-Digital Converter (ADC) allowing the board to generate and read analog signals. The analytical performance of the integrated wireless biosensor platform is validated by showing that electrical signals (e,g, current and voltage)

are reliably received using wireless communication to personal electronic devices,

laptops and smartphones, for further analysis and reporting.

4.3. Description of SNP Detection Using Fluorescence-Based Observations of DNA nano-tweezers activity

The scheme of strand displacement and single mismatch detection is shown in Fig. 1.

DNA nano-tweezers are prepared by the hybridization of two complementary strands.

Both normal and weak strands (N and W) are 57 nt. N and W consisted of zipper, loop

and hinge parts. The zipper and hinge parts are complementary and hybridized each other,

while the loop parts are non-complementary and remained un-hybridized. Therefore, N

and W are complementary to each other except 10 nt of loop part in the middle of the

DNA nano-tweezers. W contains 4 guanines which are substituted with inosines (I) to

lessen the affinity between the two strands. The structure of the DNA nano-tweezers with

specific sequences is shown in Fig. S2. As shown in Fig. 1, when 30 nt of target strand

(T), which is fully complementary with N and 5nt of the loop part on N, is introduced to

DNA nano-tweezers, it displaces W and hybridizes with N. Even though the

displacement happens, the hinge part is not dissociated and keeps binding with the DNA

nano-tweezers; the triple stranded complex is formed.[14c, 45-46, 60b, 66] Inosine (I) plays the

role of shortening the toehold part. When T has a single mismatch to N, the affinity

between N and T is significantly decreased and the reaction rate is greatly reduced; DNA nano-tweezers remain in its initial conformation (Fig. 1, bottom).[60b]

Strand displacement was monitored over time with fluorescence labeling (Fig. 3). A Texas Red fluorophore was labeled at the end of W and a fluorescence quencher was at the end of N. The quencher absorbed emission from the fluorescence when it was adjacent to fluorescence label, thus causing flouresence to be quenched upon the hybridization of N and W. When the perfect match T was added to the sample, strand displacement happened, separating the fluorophore and quencher, causing a brighter fluorescence signal. However, when the single mismatch T was added, strand displacement happend much slower and much lower fluorescence signals were measured compared to a perfect match T. The formation and operation of the DNA nano-tweezers with perfect match T and single mismatch T strands were also proven by DNA gel electrophoresis in the previous report.[45, 60b]

4.4. Detection of Opening of DNA nano-tweezers on Graphene FET

A graphene FET with two electrodes and a liquid gate chamber was fabricated to examine electrical sensing of DNA using DNA nano-tweezers-based probes (Fig. 1). The toehold part of N, located in the loop part which is adjacent to the graphene surface (Fig. 1B, black dotted circle), became double-stranded after the opening of DNA nano-tweezers by strand displacement. This changed the electrical signals as shown in the I-V curve and the corresponding electrical resistance. DNA strand displacement-based probe

namely, double stranded probe (DS probe) was reported to enhance the specificity of the DNA detection.[60b] Importantly, unlike the DS probe, DNA nano-tweezers-based probe has more complex structure, and the center of the probe is attached to the graphene surface. Therefore, causing DNA nano-tweezers to not stand up on the surface, but instead lay down on it. When it was open, the triple stranded structure pushes the detecting portion closer to the surface resulting in a signal which is larger than it was for the DS probe. Comparison of the two different probes is described in Fig. 4. Graphene chip fabrication and the probe immobilization followed the published methods.[60b]

The graphene after transfer was characterized by Raman microscopy. The Raman spectrum of the graphene sample indicated high-quality monolayer graphene, as it shows typical Raman spectrum of a single layer graphene (Fig. 5A).[67] Structural features of the functionalized graphene surface were imaged by Atomic Force Microscopy (AFM). The graphene in Fig. 5B shows a flat surface with some wrinkles of about 1-2 nm in height. Upon immobilization on the graphene, the DNA nano-tweezers appear as globular structures with an average height of 3.7 ± 0.7 nm with features between $\sim$2-8 nm (Fig. 5C) and are in good agreement with previously published data.[60b] The DNA nano-tweezers in the fluid medium stand up vertically (Fig. 1B) but lie down horizontally in the air (Fig. 5E). AFM image of the graphene without DNA nano-tweezers in air is shown in Fig. S3. After addition of the perfect match DNA, the height of the globular structures decrease slightly to 3.5 ± 0.8 nm but the diameter increases significantly, from 17.6 ± 3.3 nm for the unbound probe to 21.8 ± 5.0 nm for the probe with the perfect match DNA (Fig. 5D). This observation is consistent with the fact that the newly bound strand adds to the size of the structure, which, along with steric repulsion between the

different strands, results in a broader overall shape. The binding of the perfect match

DNA could hence be confirmed by AFM. The results indicate that the graphene on the

fabricated FET sensor chip is a monolayer and supports the functionalization strategy for

the complex design of DNA nano-tweezers.

Effect of the strand displacement was measured using a 12.5 mM MgCl2 and 30 mM Tris

buffer. The electrical effect of DNA is reported to be rapidly decreased, and only a few

sequences that are close to the graphene surface determine the electrostatic potential on

the sensor. Thus, the first few sequences would have effective charges on the surface.[55]

Importantly, the loop part of the DNA nano-tweezers is fixed to the surface of the

graphene, while the sensing part is laid down to the surface, enabling effective detection.

To examine the specificity of the graphene FET sensor, perfect match and single-

mismatch samples were tested. Target strands in concentrations from (100 nM to 100 μM

were incubated on the sensor overnight (Fig. 6). When the perfect-match T was used on

the graphene sensor, the U-shaped I-V curve shifted down and to the left, which indicates

increasing resistance and imposition of the n-doping effect.[18, 60b] The corresponding

resistance change was observed as discussed below. As the concentration of target

strands increased, DS probe showed clear discrimination of single mismatch (Fig. 6). As

the concentration of the perfect-match T was increased, I-V curve kept shifting left and

down and the shape of the curve became flatter. As shown in the Fig. 6C, the Dirac point

of the I-V curve was shifted approximately by −15 mV with 100 nM and by −95 mV with

10 μM of perfect-match T while approximately by −2 mV for both 100 nM and 10 μM of

single-mismatch T (7.5-fold and 47.5-fold difference each).

Compared to the previous study using double-stranded probe, the difference at the equivalent experimental condition were ~3-fold and ~4.3- fold. The differences achieved by using DNA nano-tweezers is more than 10 times larger than those achieved by using double-stranded probes in the previous report. We reason that this is due to the vertically standing formation of the DNA nano-tweezers probe (Fig. 4). The single-mismatch T made much smaller shift.[60b] It is reasonable to believe that a single-mismatch T could not result in the proper strand displacement, whereas a perfect-match T could induce a proper strand displacement.

The resistance change was measured for the perfect-match and the single-mismatch targets at different concentrations (Fig. 6). When DNA is accumulated on the graphene surface, its resistance increases. As shown in the Fig. 6C, perfect-match T increased the resistance significantly more than single-mismatch T. Clear differences were observed at all the target concentrations from 100 nM to 100 μM and it shows much clearer discrimination of the single mismatch compared to previous work.[60b] After measurements on the probe station, the resistance was measured with wireless signaling. The data from the two measurement systems were well matched with ~ 1% difference. The setup process for the wireless signaling is described in the following sections. The screenshot of the data received by smartphone is shown in Fig. 2A.

4.5. Generation of Wireless Signal

The FRDM-KL25Z microcontroller board can generate a digital approximation of an analog signal using pulse-width-modulation (PWM). Typically, PWM signals give a

relatively good representation of an analog signal because most electronic appliances do not react to relatively small voltage changes[68]. However, because of the electrolysis of aqueous solutions, the graphene system is sensitive to significant voltage changes. The microcontroller board creates the PWM signal by switching the voltage digitally (between only two modes) off (0 V) and on (3.3 V) producing an analog signal determined by the time averaging 0 V and 3.3 V over each period interval. For example, to produce a PWM analog signal of 1 V, the microcontroller board generates a signal of 0 V for 70 % of the time and 3.3 V signal for 30 % of the time. The nature of PWM signals can therefore cause the DNA-chip to experience a voltage of 3.3V regardless of how small the 'analog' signal generated by the microcontroller board. This bias voltage can cause electrolysis of the aqueous electrolytes and its effect on the system is evident in I-V plot of the system before low-pass filtering (Fig. 7A). The effect from the 3.3 V spikes was removed from the system by implementing a simple 1st order Resistance-Capacitor (RC) low-pass filter with the shown configuration used (Fig. S4).[69]

An RC filter is characterized by its time constant (τ) which is defined as the time required to charge the capacitor to the fraction 1/e of its maximum charge.[70] Low-pass RC filter was constructed using a 5 kΩ resistor and a 33 nF capacitor (calculations are presented in supporting materials). Initially, giving a measurement of $V_{out} = 0.1$ V. However, as illustrated by cursors A and B in Fig. S5, V_{out} varies from 0.176V to 0.064V. This huge range of V_{out} values is undesirable as the graphene FET should be subjected to a more constant voltage. This can be achieved by increasing the time constant of the RC filter. The RC filter used in this study has a 10 kΩ, resistor and a 33 nF capacitor. Fig. S6

shows that these RC values reduced the range of V_{out} to 0.14 V - 0.084 V. This configuration gave the same DMM measurement of $V_{out} = 0.1V$ as the previous RC filter but with a smaller V_{out} variation. Specific calculations for the low pass filter are in the supporting materials.

The RC filter acted as a Digital-to-Analog converter (DAC) to the PWM signal generating a V_{out} of 0.1V. Filtering reduced the peak voltage experienced by the graphene FET to 0.14V instead of the original 3.3V. Resistance of DNA attached graphene FET was measured and illustrated in Fig. 7B. The results suggest that the aqueous electrolyte system and DNA attached to the graphene surface is stable from detachment.

4.6. Evaluation of Measurement System

The FRDM-KL25Z microcontroller board provides 5 analog-to-digital converters (ADC) to measure analog signals. The board can only measure voltages; therefore, requires currents to be converted into voltage signals before it can be measured. In this application, currents over a range of voltages were recorded to examine the resistance of graphene FETs. Currents were converted to voltages by using a 1 kΩ pull-up resistor between the graphene FET and the ground. The voltage across the resistor was then measured and converted to the currents using ohm's law. These results were then plotted on a I-V graph with the gradient of the trend line representing the resistance of the entire circuit. The use of a trend line rejects measurement noise and reduces the impact of anomalous data points.

In addition, to reduce noise in the voltage measurement by the FRDM-KL25Z microcontroller board, every data point was taken as an average over 10000 samples measured. The improvement from signal averaging is shown in Fig. 7B. Measured values vary drastically when no averaging was done. To further improve the measurement accuracy, a 2nd order moving average filter was implemented using the equation presented in supporting materials, 2nd order moving average filter[71]. The filtering further improved the measured values, filtering minor measurement inaccuracies (+0.35 %); calculations are in the supporting materials.

4.7. Post Measurement Processing

Root Mean Squared Error (RMSE) was used as the measure of accuracy, with smaller RMSE values corresponding to a better accuracy. From Fig. S7, data without further processing shows an average RMSE of 260.7 while average RMSE of processed data is 171.4 giving a 34.25% improvement in the accuracy. By nature of this algorithm, more accurate data points result in an increased accuracy for each 1000-sample blocks. This is because more accurate data points allow better modeling of the measurement noise levels to be removed from device measurements. This is evident in Fig. S7 where RMSE for the first few blocks is relatively high and fluctuates drastically. As the number of accurate data points increases to 11, RMSE values start to decrease and stabilize.

Using the wireless setup, the data was transferred to both personal computer and smartphone. The example of the screenshot is shown in Fig. 3A and Fig. S8. Electrical detection of biomolecule can substitute the current fluorescence-based microarray, which

would lead to better accessibility to patients. It also can contribute to end-user-friendly platforms such as wearable or implantable biosensor. For those purposes, enhancement of specificity and wireless communication capability addressed in this paper are essential. As such, the further development and implementation of those technology would allow more affordable and accurate diagnosis of diseases including cancer and degenerative, genetic, and other various disorders.

4.8. Conclusion

Probe-less DNA detection with single-nucleotide resolution was successfully demonstrated using graphene transistor, DNA nano-tweezers-based device and wireless communication. The Dirac point and resistance of the channel on the graphene FET sensor changed when DNA nano-tweezers-based probe was opened by target DNA strands on the graphene surface. Due to the intelligent design of the functional DNA nano-tweezers, the signal ratio was enhanced compared to the previous report using DNA zippers. Electrical signals generated by biosensors, such as current and voltage, were transmitted for further processing to personal electronic devices, laptops and smartphones, using real-time wireless communication. This work contributes to the practicality of electrical-based (label-free) nucleic acid sensors by improving the portability of the sensor and the accessibility between nano-devices monitoring biomolecular nano-systems with end-user electronic devices. The present wireless biosensor platform will facilitate the development of implantable, digitalized, and wireless biosensors for early detection and continuing real-time therapy efficacy monitoring of potentially life threatening human diseases.

4.9. Materials and Methods

4.9.1. Materials

Conducting silver paste was obtained from Sigma Aldrich (Saint Louis, MO). Chemical vapor deposition (CVD) grown graphene was purchased from ACS material (Medford, MA). Silicone rubber was purchased from Dow Corning (Midland, MI). PBS solution was purchased from Thermo Fisher Scientific (Waltham, MA). Poly (methyl methacrylate) (PMMA) was purchased from MicroChem (Westborough, MA). DNA gels were purchased from Lonza (Walkersville, MD). Ultrapure water was obtained from a Millipore A10 water purification system and had a resistance of 18.2 MΩ. The FRDM KL-25Z microcontroller board was purchased from Freescale Semiconductor, Inc. A Bluetooth HC-06 module was purchased from Guangzhou HC Information Technology Co., Ltd. All DNA oligonucleotides were purchased from IDT (Coralville, IA) and all DNA sequences are listed in supporting materials (Table S1).

4.9.2. Fluorescence Test

The normal strand (N) side, which was tagged with fluorescence quencher, and the weak strand (W) side, which was tagged with fluorescence label, are mixed in a ratio of 1:1 in 1× PBS solution and annealed from 20 to 90 °C and cooled to 4 °C over 4 h. Texas red has an excitation maximum wavelength of 596 nm and an emission maximum wavelength of 613 nm. Perfect-match and single-mismatch T strands are all suspended in 1× PBS. The hybridized DS probe was diluted in 1× PBS and tested using a Tecan

Infinite 200 M plate-reading spectrometer at 27 °C, with an accuracy we estimate to be

approximately ±1.5 °C. Excitation and emission of Texas red are observed at 590 and 620

nm, respectively. Each experiment began with a 50-µL sample volume with a device

concentration of 20 nM (20 nM DNA tweezers and 100 and 300 nM T) in black 96-well

plates. Clear microplate sealing films were applied over the sample wells to avoid

evaporation.

4.9.3. Fabrication of Graphene FET Chip

The graphene film was cut into ~ 2 mm × 7 mm size with scissors. Graphene

films were obtained from the maker prepared on thin copper substrates. The graphene

was on the both side of the copper foil and only the top side was used for FET fabrication.

To separate the graphene from the copper substrate PMMA was spin-coated on the top

(carbon) surface of graphene/copper substrate to protect the graphene while the copper

bottom was etched away. Copper was etched by floating on 0.1 M of ammonium

persulfate for about 5 hours and rinsed in deionized (DI) water overnight. PMMA acted

as a supporting layer to the graphene once the copper was etch away. The back side of

graphene was removed by oxygen plasma etching. The graphene supported by PMMA

was then transferred onto a silicon dioxide coated wafer followed by removal of the

PMMA layer with acetone at 60 °C for 1 hour. The sample was then annealed at 300 °C

for 2 hours under hydrogen/argon atmosphere[57]. To fabricate a transistor, conducting

silver paste was used as source and drain electrodes at two ends of the graphene. Silicone

rubber was then applied to insulate source and drain electrodes from liquid and also used

as a solution reservoir.

4.9.4. Immobilization of DNA tweezers

PASE (5 mM) in dimethylformamide (DMF) was treated on graphene for 1 h and rinsed with pure DMF and DI water; 50 µM of DS probe was added on PASE-modified graphene for 2 h. The graphene FET with DS probe functionalization was rinsed with 1× PBS; 100 mM ethanolamine solution was treated to saturate the possibly unreacted amino group on PASE and rinsed with 1× PBS solution. The volume of all treated chemicals and samples was 40 µL.

4.9.5. Visualization of DNA and Graphene Surface

Topographic images of DNA on graphene surface were acquired using a Multimode AFM equipped with a Nanoscope V controller (Bruker). Silicon cantilevers with a spring constant of 42 N/m (PPP-NCHR; Nanosensor) were used for imaging in air using tapping mode. Silicon nitride cantilevers with spring constants of 0.08 N/m (OMCLTR400; Olympus) were used for imaging in fluid using peak force-tapping mode. Nanoscope Analysis 1.50 was used for analyzing imaged data.

4.9.6. Strand Displacement on the Chip

The strand displacement reaction was conducted by dropping perfect-match and single-mismatch T strands with concentrations that are indicated in the legends in Figure 5 of data and incubated overnight in the reservoir on the graphene FET chip. Then, the chip was rinsed gently with 1× PBS. All of the volume of treated samples was 50 µL.

4.9.7. Electrical Measurements

I-V curves and resistance were measured in a semiconductor parameter analyzer equipped with a probe station. Silver wire was used as an electrode, which applied gate voltage (Vg) to the 12.5 mM MgCl2/30 mM Tris buffer solution. Tests were also conducted with 1× PBS buffer solution. Vg was swept from −0.5 to 1 V, and drain–source voltage (Vds) was picked between 0.05 and 0.3 V. Drain–source current (Ids) was measured at an assigned Vds. Resistances were measured between 0 ~ 100 mV of Vds. After measurements on the probe station, resistance measurements were simultaneously performed using a standard digital multi-meter (DMM) (Fluke 175 True RMS multimeter) and a smartphone connected via the wireless system. The source voltage was swept between 0 and 0.5 V. Current values were converted into a voltage signal by introducing a pull-up resistor of 1 kΩ. The potential difference which corresponds to 1000 times the current value was measured by the device. This data was sent to a smartphone for further data processing. Voltage values were plotted against their respective current values with a trend line. Gradient of the trend line represents resistance of the entire circuit with the resistance of device obtained by subtracting the resistance of the other components, 1 kΩ pull-up resistor and 10 kΩ filtering resistor.

4.9.8. Wireless Communication

Communication was established through the HC-06 Bluetooth module.[70a] The HC-06 module communicated with the FRDM-KL25Z using the Serial RS-232 communication protocol while pairing with user electronics, phones and computers, over

the Bluetooth communication standard (Figure 2). The HC-06 module supports Bluetooth communication baud rates up to 115200 bps, a baud rate of 9600bps was used for communication with the smartphone device.

Chapter 4 is a publication in preparation. Hwang M. T., Shiah Z. C., Antonschmidt L., Lee. J., Glinsky G., Lal R. Wireless communication of label-free SNP detection using 2-D electronics and DNA nano-tweezers. The dissertation author is a primary author.
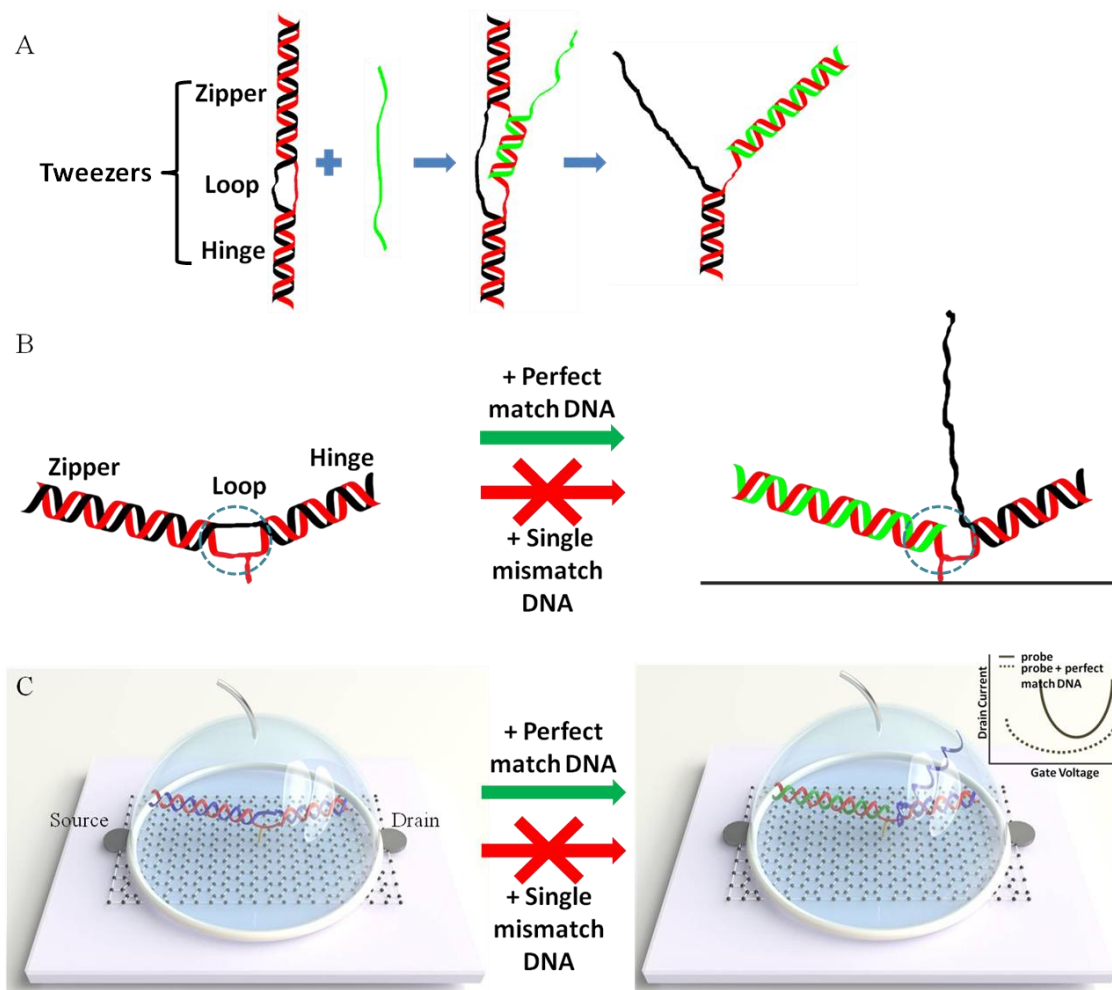
Figure 4.1. Schematics of the DNA nano sensors. (A) DNA nano-tweezers action. The red strand is the normal strand (N) containing 10 nt of loop. When the perfect-match target strand (green strand) approaches a DNA tweezers, the target strand displaces the weak strand (W) (black strand) by binding to the loop. The tweezers are bound by the hinge, thus forming a triple-stranded complex. (B) DNA tweezers probe action, which is horizontally immobilized on the graphene surface. The green strand displaces the black strand, and part of the loop portion becomes double-stranded (blue dotted circle region). As three DNA parts are dangling, the occupied loop part is located close to the surface due to the steric effect. (C) Graphene FET sensor with DNA tweezers probe. Gate voltage is applied directly on the liquid gate; the liquid gate is shown as a hemisphere (light blue) surrounding the DNA tweezers probe. A target strand with single mismatch does not allow the strand displacement properly. Thus, the toehold region remains single-stranded (blue dotted circle in B, Left). The inset shows I-V relationship (I-V curve) attributable to charge difference during the strand displacement in the gene chip FET sensor. The I-V curve shifts leftward and downward. Single-mismatch target strand does not displace the black strand properly; thus, the I-V curve remains almost the same.
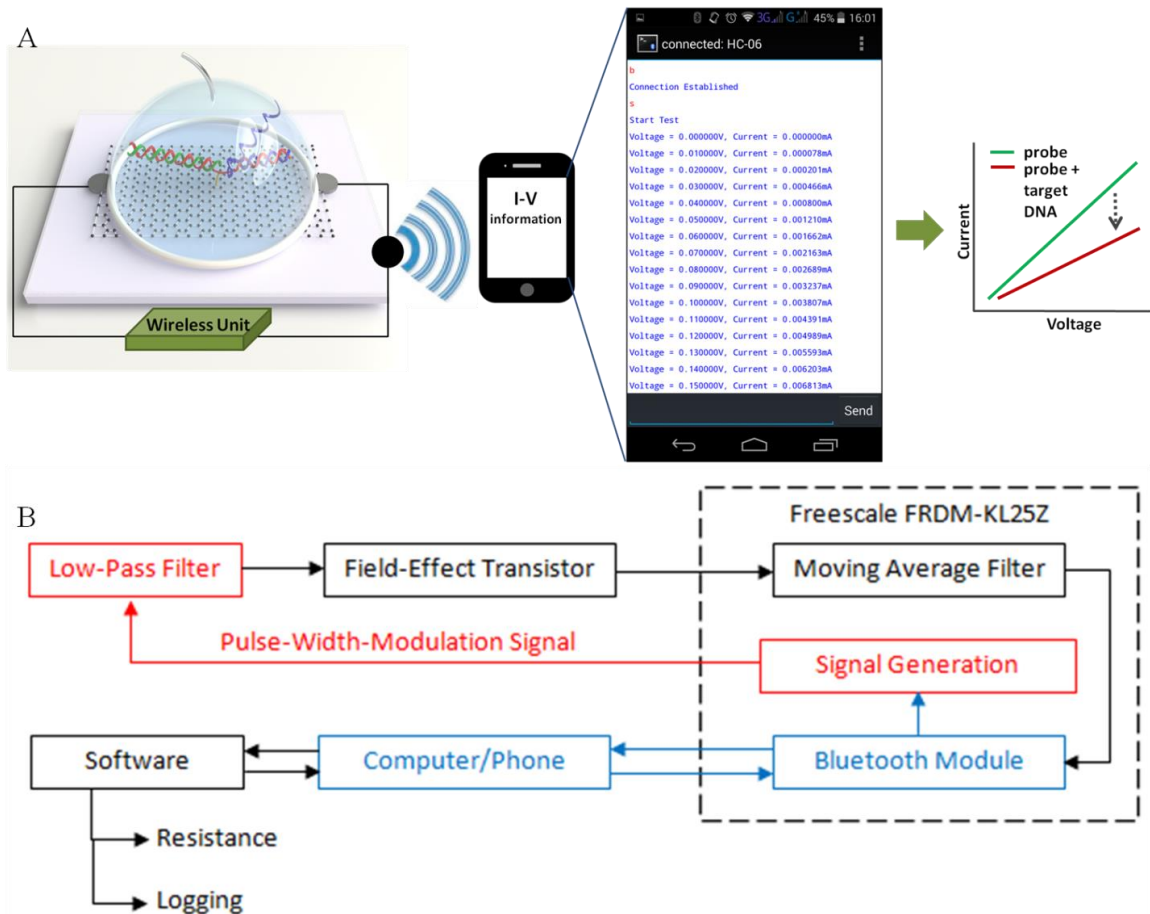
Figure 4.2. The schematics of the data transmission from the biosensor chip to a smartphone.
Electrical voltage and current data are transmitted to a smartphone for further processing to obtain resistance values. The magnified screenshot of Bluetooth terminal shows data received by the Smartphone during a test demonstrating communication between device and phone. The data is interpreted as I-V graph which shows resistance changes before and after the detection of DNA. B) Top-level design of the device with different operation modules highlighted. (Blue: Communication, Red: Signal Generation, Black: Measurement)

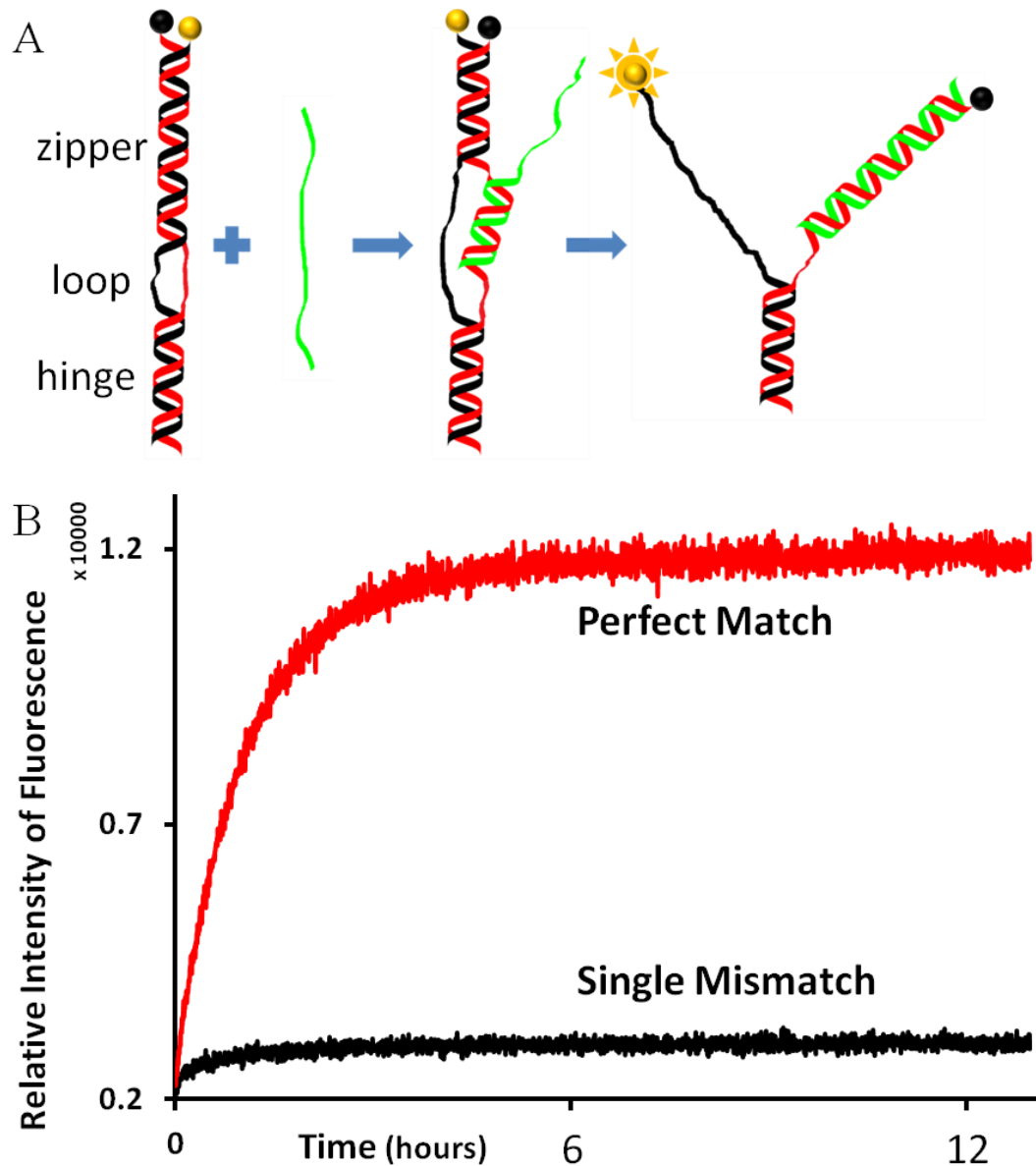**Figure 4.3. Single-mismatch detection using fluorescently labeled DNA tweezers.** (A) Schematics of strand displacement: nucleotide with fluorophores (yellow ball) and nucleotide with quencher (black ball). Initially, the normal (N) (red) and weak (W) (black) strands are hybridized; fluorophore (yellow ball) and quencher (black ball) are adjacent so that fluorescence is quenched. When the green strand (perfect-match T) interacts with DNA tweezers, strand displacement takes place, causing N and perfect-match target strand to hybridize. Though W is bound by hinge, it is away from the N and the fluorophore becomes active. (B) Real-time fluorescence measurement of the strand displacement. Interaction of the single-mismatch target strand with DNA tweezers show much less fluorescence activity than the interaction of the perfect match with DNA tweezers. The concentration of DNA tweezers was 20 nM, and the concentration of T strand is 100 nM.
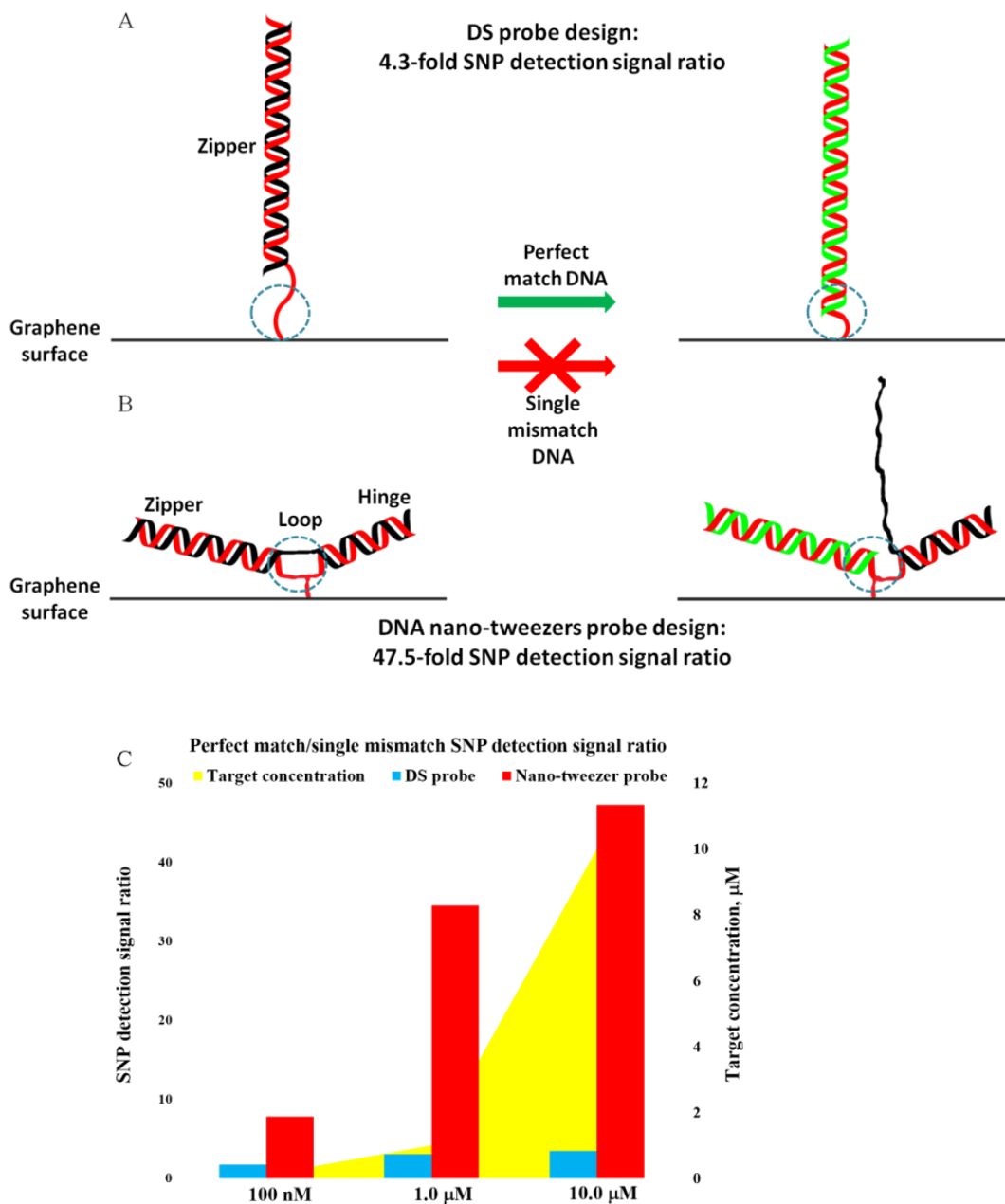
Figure 4.4. Comparison of the two probe designs, double-stranded (DS) probe and DNA nano-tweezers probe. (A) Previously reported probe DS probe design.[13] The green strand displaces the black strand, and the toehold portion becomes double-stranded, thus more charges from DNA are accumulated and detected. The probe is vertically standing up on the graphene surface. As the electrical effect of DNA is reported to be rapidly decreased with distance, and only a few nucleotides (light blue dot circle) that are close to the graphene surface determine the electrostatic potential on the sensor. [31] (B) DNA nano-tweezers probe design engineered in this work. As the probe is horizontally laid down on the graphene surface, the charge accumulation part (the loop within the light blue dot circle) is closely located to the graphene surface. When the green strand displaces the black strand, the part of the hinge part becomes double-stranded. Because the longer DNA sequences of the charge accumulation part are positioned closer to the surface than in the DS probe, it gives the larger signal. (C) Comparisons of the perfect match/single

nucleotide mismatch SNP detection signal ratios in the physiologically-relevant range of target concentrations.
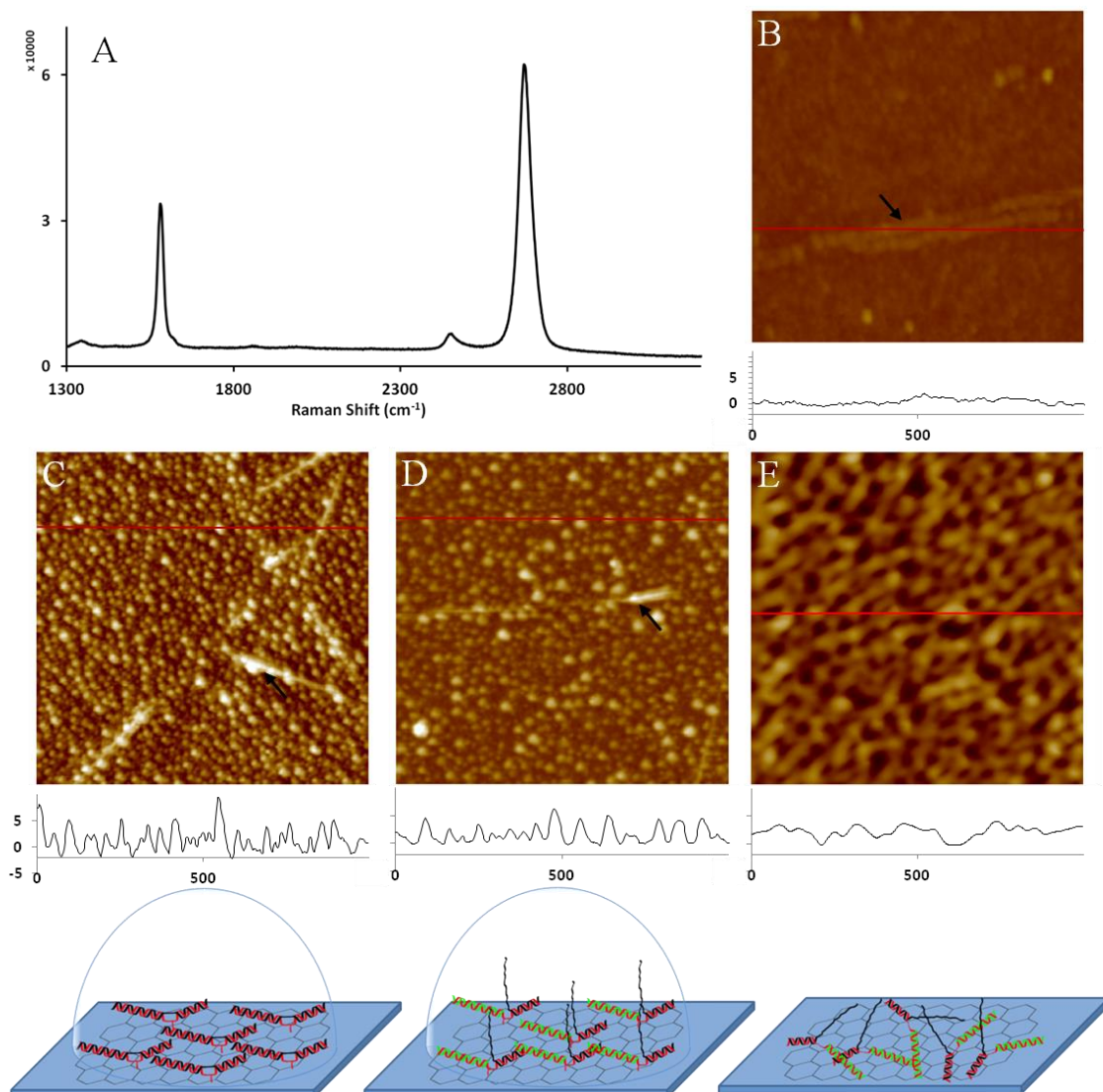

Figure 4.5. Raman spectrum of the graphene and AFM images of graphene transistor surface with and without the DNA sensor. (A) Raman spectrum of the CVD graphene, indicating that the transferred graphene was a single layer. (B) The graphene surface in fluid is mostly flat with some wrinkles. (C) Graphene surface covered with DNA tweezers in fluid, strands produce features of ~2-8 nm in height with an average diameter of about 18 nm. (D) After binding of a perfect match DNA strand in fluid the features decrease slightly in height to about ~2-6 nm and increase in diameter to about 22 nm. (E) AFM images of graphene transistor surface with the DNA sensor in air. When not surrounded by fluid medium, the DNA tweezers linked to graphene lie down on the surface in random polygonal patterns. Black arrows indicate graphene wrinkles. Cartoons at the bottom represent models of formation of DNA structure in liquid and air. All images have a scan area of 1 × 1 μm and a z range of 19 nm. All the units in the surface height profiles are nm.

Perfect match T: 5'- TAA TAA TAG AAT TTT AAA AGA CTG GAA TAA -3'
Single mismatch T: 5'- TAA TAA TAG AA*G* TTT AAA AGA CTG GAA TAA -3'
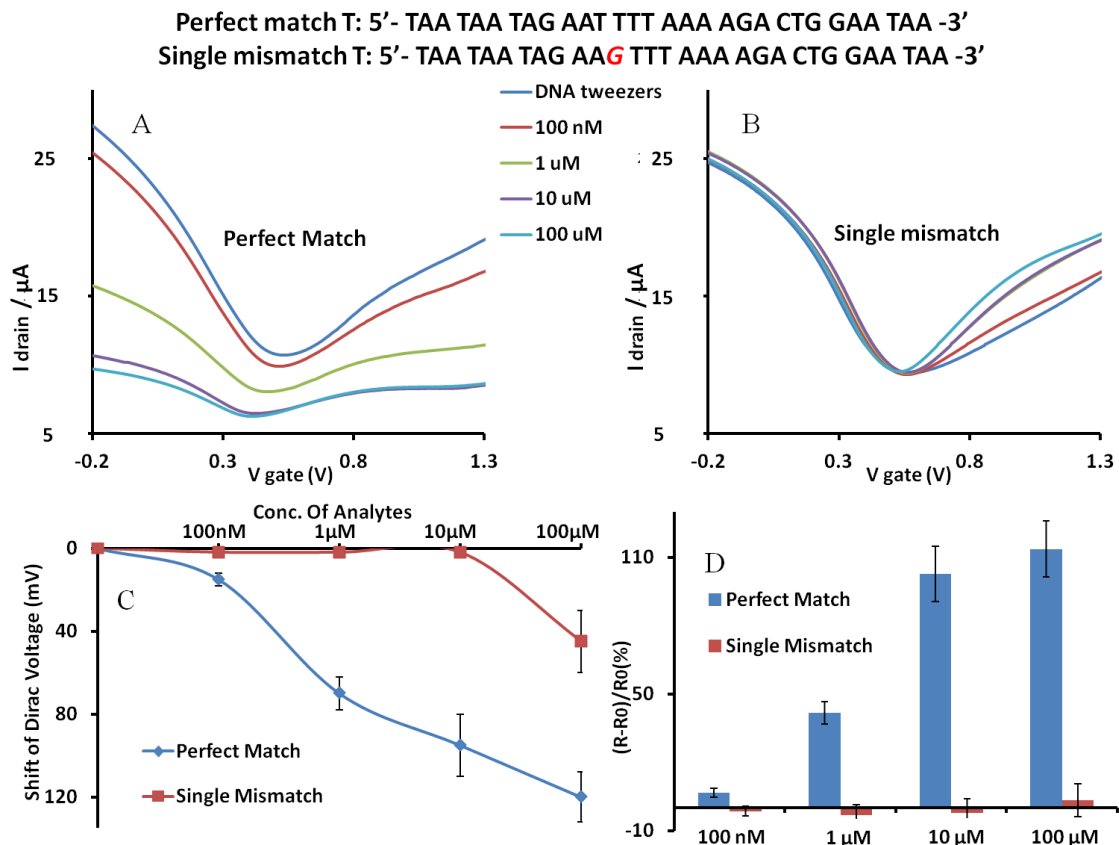
Figure 4.6. -V relationship of the graphene FET sensor for the strand displacement reactions. (A) The perfect-match T shifted the I-V curve according to the indicated concentrations. (B) The single-mismatch T shifts the I-V curve significantly less. The DNA sequences of T used in the experiments are shown over the I-V curve. (C) Dirac voltage shift of the FET sensor. The Dirac voltage is expressed as a function of the concentration of the added target DNAs. (D) Distinguishable resistance changes of the channel layer caused by strand displacement at different concentrations of the T DNAs.

Figure 4.7. I-V graphs depends on various filter conditions. (A)I-V graphs comparing resistance changes when DNA is added, before and after low-pass filtering is performed. When the measurements were done without passing the PWM signal through a low-pass Filter, similar resistance values, 0.0038MΩ and 0.004MΩ, illustrate the detachment of DNA from graphene surface regardless of how small the 'analog' signal generated by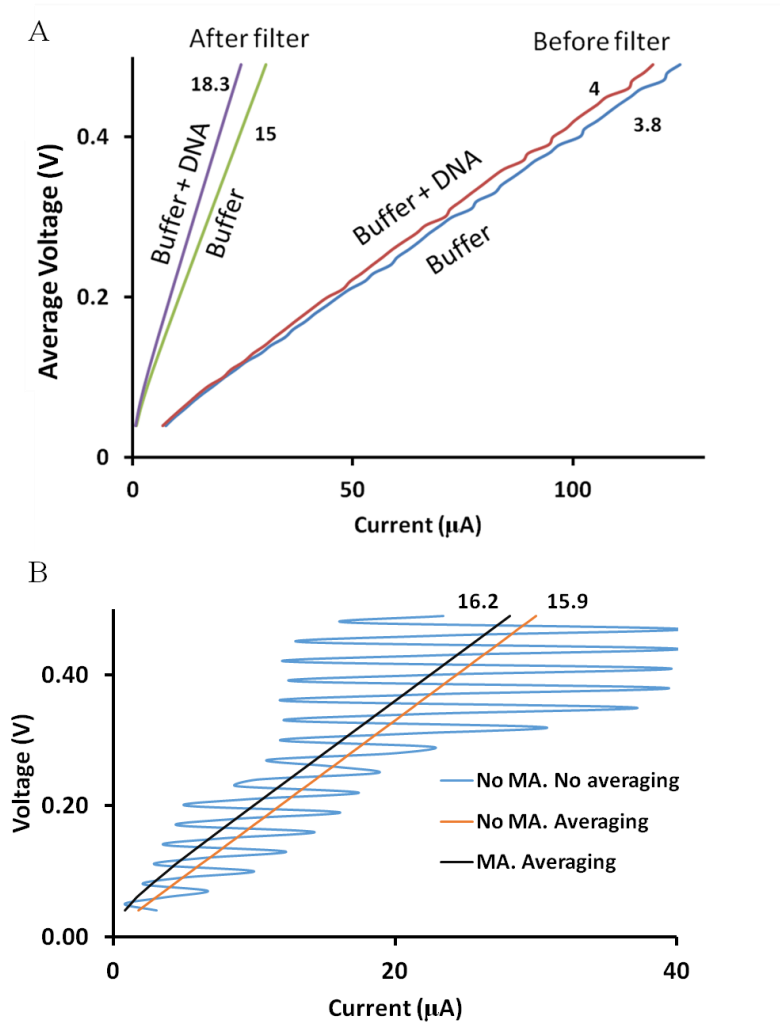 the device is. This is due to the nature of PWM signals, subjecting the DNA to 3.3V regardless of the 'analog' signal generated. When the measurements were done after passing the PWM signal through a low-pass filter, the change in resistance values, 0.0183MΩ to 0.015MΩ is more significant as compared to that without low-pass Filtering. This implies that applying a voltage of 3.3V caused DNA to detach from the graphene surface. Filtering is implemented in this device to ensure accurate measurement. RC low-pass filter with τ = 330μs used. Numbers beside lines represent resistance in kΩ. (B) I-V curve of 5k resistor measured by the device before and after applying the various filtering techniques, averaging of 10000 samples taken and a 2nd order Moving-Average filter. Filtering techniques show huge improvements in measurement accuracy. Final device design has both averaging and the Moving-Average filter implemented. Gradient of the trend line of the data points corresponds to resistance. Device measured a total resistance of 0.0162 MΩ and 0.0159 MΩ. Removing the resistance contributions from the low-pass filter and sense resistor gives a measured resistance of 5.2 kΩ and 4.9 kΩ respectively. Numbers above lines represent resistance in kΩ.

Table 4.1. Resistance values measured by device and specialized equipment and changes in estimated measurement noise

Data Points	1	2	3	4	5	6	7	8	9
Device(Ω)	3894.4	5059.8	4775.9	3916.9	7320	3413.2	2038.5	3644.3	5883.4
Accurate(Ω)	3780	4980	4850	3780	7080	3210	1850	3440	5800
Noise	1.0303	1.0160	0.9847	1.0362	1.0339	1.0633	1.1019	1.0594	1.0144
E(Noise)	1.0303	1.0231	1.0103	1.0168	1.0202	1.0274	1.0380	1.0407	1.0378

Bibliography

1.   Barany, F., Genetic disease detection and DNA amplification using cloned thermostable ligase. *Proceedings of the National Academy of Sciences* **1991,** *88* (1), 189-193.

2.   Shapiro, J., Genome Informatics: The Role of DNA in Cellular Computations. *Biol Theory* **2006,** *1* (3), 288-301.

3.   Jin, L.; Chakraborty, R., Population structure, stepwise mutations, heterozygote deficiency and their implications in DNA forensics. *Heredity* **1995,** *74* (3), 274-285.

4.   Wang, J.; Rivas, G.; Cai, X.; Palecek, E.; Nielsen, P.; Shiraishi, H.; Dontha, N.; Luo, D.; Parrado, C.; Chicharro, M.; Farias, P. A. M.; Valera, F. S.; Grant, D. H.; Ozsoz, M.; Flair, M. N., DNA electrochemical biosensors for environmental monitoring. A review. *Analytica Chimica Acta* **1997,** *347* (1), 1-8.

5.   (a) Singh, M.; Singh, P.; Juneja, P.; Singh, S.; Kaur, T., SNP–SNP interactions within APOE gene influence plasma lipids in postmenopausal osteoporosis. *Rheumatol Int* **2011,** *31* (3), 421-423; (b) Kujovich, J. L., Factor V Leiden thrombophilia. *Genet Med* **2011,** *13* (1), 1-16; (c) Wolf, A. B.; Caselli, R. J.; Reiman, E. M.; Valla, J., APOE and neuroenergetics: an emerging paradigm in Alzheimer's disease. *Neurobiology of Aging* **2013,** *34* (4), 1007-1017.

6.   Jain, K. K., Personalized medicine. *Curr Opin Mol Ther* **2002,** *4* (6), 548-558.

7.   Newton, C. R.; Graham, A.; Heptinstall, L. E.; Powell, S. J.; Summers, C.; Kalsheker, N.; Smith, J. C.; Markham, A. F., Analysis of any point mutation in DNA. The amplification refractory mutation system (ARMS). *Nucleic Acids Research* **1989,** *17* (7), 2503-2516.

8.   Olivier, M., The Invader® assay for SNP genotyping. *Mutation Research/Fundamental and Molecular Mechanisms of Mutagenesis* **2005,** *573* (1–2), 103-110.

9.   (a) Schena, M.; Shalon, D.; Davis, R. W.; Brown, P. O., Quantitative Monitoring of Gene Expression Patterns with a Complementary DNA Microarray. *Science* **1995,** *270* (5235), 467-470; (b) Lashkari, D. A.; DeRisi, J. L.; McCusker, J. H.; Namath, A. F.; Gentile, C.; Hwang, S. Y.; Brown, P. O.; Davis, R. W., Yeast microarrays for genome wide parallel genetic and gene expressionâ€‰analysis. *Proceedings of the National Academy of Sciences* **1997,** *94* (24), 13057-13062.

10.   Rapley, R.; Harbron, S., *Molecular analysis and genome discovery*. Wiley Online Library: 2004.

11.   (a) Tyagi, S.; Kramer, F. R., Molecular Beacons: Probes that Fluoresce upon Hybridization. *Nat Biotech* **1996,** *14* (3), 303-308; (b) Xiao, Y.; Lou, X.; Uzawa, T.; Plakos, K. J. I.; Plaxco, K. W.; Soh, H. T., An Electrochemical Sensor for Single Nucleotide Polymorphism Detection in Serum Based on a Triple-Stem DNA Probe. *Journal of the American Chemical Society* **2009,** *131* (42), 15311-15316; (c) Xiao, Y.; Plakos, K. J. I.; Lou, X.; White, R. J.; Qian, J.;

Plaxco, K. W.; Soh, H. T., Fluorescence Detection of Single-Nucleotide Polymorphisms with a Single, Self-Complementary, Triple-Stem DNA Probe. *Angewandte Chemie International Edition* **2009,** *48* (24), 4354-4358.

12.   (a) Relógio, A.; Schwager, C.; Richter, A.; Ansorge, W.; Valcárcel, J., Optimization of oligonucleotide-based DNA microarrays. *Nucleic Acids Research* **2002,** *30* (11), e51; (b) Hughes, T. R.; Mao, M.; Jones, A. R.; Burchard, J.; Marton, M. J.; Shannon, K. W.; Lefkowitz, S. M.; Ziman, M.; Schelter, J. M.; Meyer, M. R.; Kobayashi, S.; Davis, C.; Dai, H.; He, Y. D.; Stephaniants, S. B.; Cavet, G.; Walker, W. L.; West, A.; Coffey, E.; Shoemaker, D. D.; Stoughton, R.; Blanchard, A. P.; Friend, S. H.; Linsley, P. S., Expression profiling using microarrays fabricated by an ink-jet oligonucleotide synthesizer. *Nat Biotech* **2001,** *19* (4), 342-347.

13.   Zhang, D. Y.; Seelig, G., Dynamic DNA nanotechnology using strand-displacement reactions. *Nature chemistry* **2011,** *3* (2), 103-113.

14.   (a) Khodakov, D. A.; Khodakova, A. S.; Linacre, A.; Ellis, A. V., Toehold-Mediated Nonenzymatic DNA Strand Displacement As a Platform for DNA Genotyping. *Journal of the American Chemical Society* **2013,** *135* (15), 5612-5619; (b) Matsumoto, K.; Nakata, E.; Tamura, T.; Saito, I.; Aizawa, Y.; Morii, T., A Peptide Nucleic Acid (PNA) Heteroduplex Probe Containing an Inosine–Cytosine Base Pair Discriminates a Single-Nucleotide Difference in RNA. *Chemistry – A European Journal* **2013,** *19* (16), 5034-5040; (c) Mo, A. H.; Landon, P. B.; Meckes, B.; Yang, M. M.; Glinsky, G. V.; Lal, R., An on-demand four-way junction DNAzyme nanoswitch driven by inosine-based partial strand displacement. *Nanoscale* **2014,** *6* (3), 1462-1466; (d) Hwang, M. T.; Landon, P.; Lee, J.; Mo, A. H.; Meckes, B.; Glinskii, G.; Lal, R., DNA Nano-Carrier for Repeatable Capture and Release of Biomolecules. *Nanoscale* **2015**.

15.   Yurke, B.; Turberfield, A. J.; Mills, A. P.; Simmel, F. C.; Neumann, J. L., A DNA-fuelled molecular machine made of DNA. *Nature* **2000,** *406* (6796), 605-608.

16.   Seelig, G.; Soloveichik, D.; Zhang, D. Y.; Winfree, E., Enzyme-Free Nucleic Acid Logic Circuits. *Science* **2006,** *314* (5805), 1585-1588.

17.   Zhang, Z.; Zeng, D.; Ma, H.; Feng, G.; Hu, J.; He, L.; Li, C.; Fan, C., A DNA-Origami Chip Platform for Label-Free SNP Genotyping Using Toehold-Mediated Strand Displacement. *Small* **2010,** *6* (17), 1854-1858.

18.   Cai, B.; Wang, S.; Huang, L.; Ning, Y.; Zhang, Z.; Zhang, G.-J., Ultrasensitive Label-Free Detection of PNA–DNA Hybridization by Reduced Graphene Oxide Field-Effect Transistor Biosensor. *ACS Nano* **2014,** *8* (3), 2632-2638.

19.   Souteyrand, E.; Cloarec, J. P.; Martin, J. R.; Wilson, C.; Lawrence, I.; Mikkelsen, S.; Lawrence, M. F., Direct Detection of the Hybridization of Synthetic Homo-Oligomer DNA Sequences by Field Effect. *The Journal of Physical Chemistry B* **1997,** *101* (15), 2980-2985.

20.   Ko, J. W.; Woo, J.-M.; Jinhong, A.; Cheon, J. H.; Lim, J. H.; Kim, S. H.; Chun, H.; Kim, E.; Park, Y. J., Multi-Order Dynamic Range DNA Sensor Using a Gold Decorated SWCNT Random Network. *ACS Nano* **2011,** *5* (6), 4365-4372.

21.   Gao, A.; Lu, N.; Dai, P.; Li, T.; Pei, H.; Gao, X.; Gong, Y.; Wang, Y.; Fan, C., Silicon-Nanowire-Based CMOS-Compatible Field-Effect Transistor Nanosensors for Ultrasensitive Electrical Detection of Nucleic Acids. *Nano Letters* **2011,** *11* (9), 3974-3978.

22.   Huang, Y.; Dong, X.; Shi, Y.; Li, C. M.; Li, L.-J.; Chen, P., Nanoelectronic biosensors based on CVD grown graphene. *Nanoscale* **2010,** *2* (8), 1485-1488.

23.   Mohanty, N.; Berry, V., Graphene-Based Single-Bacterium Resolution Biodevice and DNA Transistor: Interfacing Graphene Derivatives with Nanoscale and Microscale Biocomponents. *Nano Letters* **2008,** *8* (12), 4469-4476.

24.   Kwak, Y. H.; Choi, D. S.; Kim, Y. N.; Kim, H.; Yoon, D. H.; Ahn, S.-S.; Yang, J.-W.; Yang, W. S.; Seo, S., Flexible glucose sensor using CVD-grown graphene-based field effect transistor. *Biosensors and Bioelectronics* **2012,** *37* (1), 82-87.

25.   Green, N. S.; Norton, M. L., Interactions of DNA with graphene and sensing applications of graphene field-effect transistor devices: A review. *Analytica Chimica Acta* **2015,** *853*, 127-142.

26.   Ohno, Y.; Maehashi, K.; Yamashiro, Y.; Matsumoto, K., Electrolyte-Gated Graphene Field-Effect Transistors for Detecting pH and Protein Adsorption. *Nano Letters* **2009,** *9* (9), 3318-3322.

27.   Dontschuk, N.; Stacey, A.; Tadich, A.; Rietwyk, K. J.; Schenk, A.; Edmonds, M. T.; Shimoni, O.; Pakes, C. I.; Prawer, S.; Cervenka, J., A graphene field-effect transistor as a molecule-specific probe of DNA nucleobases. *Nat Commun* **2015,** *6*.

28.   Bruno, D. L.; Ganesamoorthy, D.; Schoumans, J.; Bankier, A.; Coman, D.; Delatycki, M.; Gardner, R. J. M.; Hunter, M.; James, P. A.; Kannu, P.; McGillivray, G.; Pachter, N.; Peters, H.; Rieubland, C.; Savarirayan, R.; Scheffer, I. E.; Sheffield, L.; Tan, T.; White, S. M.; Yeung, A.; Bowman, Z.; Ngo, C.; Choy, K. W.; Cacheux, V.; Wong, L.; Amor, D. J.; Slater, H. R., Detection of cryptic pathogenic copy number variations and constitutional loss of heterozygosity using high resolution SNP microarray analysis in 117 patients referred for cytogenetic analysis and impact on clinical practice. *Journal of Medical Genetics* **2009,** *46* (2), 123-131.

29.   Di, X.; Matsuzaki, H.; Webster, T. A.; Hubbell, E.; Liu, G.; Dong, S.; Bartell, D.; Huang, J.; Chiles, R.; Yang, G.; Shen, M.-m.; Kulp, D.; Kennedy, G. C.; Mei, R.; Jones, K. W.; Cawley, S., Dynamic model based algorithms for screening and genotyping over 100K SNPs on oligonucleotide microarrays. *Bioinformatics* **2005,** *21* (9), 1958-1963.

30.   (a) Täpp, I.; Malmberg, L.; Rennel, E.; Wik, M.; Syvänen, A. C., Homogeneous scoring of single-nucleotide polymorphisms: comparison of the 5'-nuclease TaqMan assay and Molecular Beacon probes. *BioTechniques* **2000,** *28* (4), 732-738; (b) Okamoto, A., ECHO probes: a concept of fluorescence control for practical nucleic acid sensing. *Chemical Society Reviews 40* (12), 5815-5828.

31.   Kolpashchikov, D. M., An Elegant Biosensor Molecular Beacon Probe: Challenges and Recent Solutions. *Scientifica 2012*, 17.

32.   Li, J. J.; Chu, Y.; Lee, B. Y.-H.; Xie, X. S., Enzymatic signal amplification of molecular beacons for sensitive DNA detection. *Nucleic Acids Research* **2008,** *36* (6), e36.

33.	Landon, P. B.; Ramachandran, S.; Gillman, A.; Gidron, T.; Yoon, D.; Lal, R., DNA Zipper-Based Tweezers. *Langmuir 28* (1), 534-540.

34.	Stockley, P. G.; Persson, B., Surface Plasmon Resonance Assays of DNA-Protein Interactions #. In *T DNA-Protein Interactions*, 2008; Vol. 543, pp 653-669.

35.	Hualin, C.; Changjian, Z.; Yihan, Z.; Yi, Y.; Tianling, R.; Cangran, G.; Jing, L. In *SAW based mass-loading biosensor for DNA detection*, Electron Devices and Solid-State Circuits (EDSSC), 2013 IEEE International Conference of, 3-5 June 2013; pp 1-2.

36.	Zhou, X. C.; Huang, L. Q.; Li, S. F. Y., Microgravimetric DNA sensor based on quartz crystal microbalance: comparison of oligonucleotide immobilization methods and the application in genetic diagnosis. *Biosensors and Bioelectronics* **2001,** *16* (1–2), 85-95.

37.	(a) Li, Z.; Chen, Y.; Li, X.; Kamins, T. I.; Nauka, K.; Williams, R. S., Sequence-Specific Label-Free DNA Sensors Based on Silicon Nanowires. *Nano Letters* **2004,** *4* (2), 245-247; (b) Fritz, J. r.; Cooper, E. B.; Gaudet, S.; Sorger, P. K.; Manalis, S. R., Electronic detection of DNA by its intrinsic molecular charge. *Proceedings of the National Academy of Sciences* **2002,** *99* (22), 14142-14146.

38.	Hahm, J.-i.; Lieber, C. M., Direct Ultrasensitive Electrical Detection of DNA and DNA Sequence Variations Using Nanowire Nanosensors. *Nano Letters* **2003,** *4* (1), 51-54.

39.	(a) Ko, J. W.; Woo, J.-M.; Jinhong, A.; Cheon, J. H.; Lim, J. H.; Kim, S. H.; Chun, H.; Kim, E.; Park, Y. J., Multi-Order Dynamic Range DNA Sensor Using a Gold Decorated SWCNT Random Network. *ACS Nano 5* (6), 4365-4372; (b) MartÃnez, M. T.; Tseng, Y.-C.; Ormategui, N.; Loinaz, I.; Eritja, R.; Bokor, J., Label-Free DNA Biosensors Based on Functionalized Carbon Nanotube Field Effect Transistors. *Nano Letters* **2009,** *9* (2), 530-536.

40.	Dong, X.; Shi, Y.; Huang, W.; Chen, P.; Li, L.-J., Electrical Detection of DNA Hybridization with Single-Base Specificity Using Transistors Based on CVD-Grown Graphene Sheets. *Advanced Materials 22* (14), 1649-1653.

41.	Chou, C.-C.; Chen, C.-H.; Lee, T.-T.; Peck, K., Optimization of probe length and the number of probes per gene for optimal microarray analysis of gene expression. *Nucleic Acids Research* **2004,** *32* (12), e99.

42.	Wang, J. S.; Zhang, D. Y., Simulation-guided DNA probe design for consistently ultraspecific hybridization. *Nat Chem* **2015,** *7* (7), 545-553.

43.	Dong, X.; Shi, Y.; Huang, W.; Chen, P.; Li, L.-J., Electrical Detection of DNA Hybridization with Single-Base Specificity Using Transistors Based on CVD-Grown Graphene Sheets. *Advanced Materials* **2010,** *22* (14), 1649-1653.

44.	Yin, Z.; He, Q.; Huang, X.; Zhang, J.; Wu, S.; Chen, P.; Lu, G.; Chen, P.; Zhang, Q.; Yan, Q.; Zhang, H., Real-time DNA detection using Pt nanoparticle-decorated reduced graphene oxide field-effect transistors. *Nanoscale* **2012,** *4* (1), 293-297.

45.	Landon, P. B.; Ramachandran, S.; Gillman, A.; Gidron, T.; Yoon, D.; Lal, R., DNA Zipper-Based Tweezers. *Langmuir* **2012,** *28* (1), 534-540.

46.   Landon, P. B.; Lee, J.; Hwang, M. T.; Mo, A. H.; Zhang, C.; Neuberger, A.; Meckes, B.; Gutierrez, J. J.; Glinsky, G.; Lal, R., Energetically Biased DNA Motor Containing a Thermodynamically Stable Partial Strand Displacement State. *Langmuir* **2014,** *30* (46), 14073-14078.

47.   Chen, T.-Y.; Loan, P. T. K.; Hsu, C.-L.; Lee, Y.-H.; Tse-Wei Wang, J.; Wei, K.-H.; Lin, C.-T.; Li, L.-J., Label-free detection of DNA hybridization using transistors based on CVD grown graphene. *Biosensors and Bioelectronics* **2013,** *41*, 103-109.

48.   Zheng, C.; Huang, L.; Zhang, H.; Sun, Z.; Zhang, Z.; Zhang, G.-J., Fabrication of Ultrasensitive Field-Effect Transistor DNA Biosensors by a Directional Transfer Technique Based on CVD-Grown Graphene. *ACS Applied Materials & Interfaces* **2015,** *7* (31), 16953-16959.

49.   (a) Calado, V. E.; Schneider, G. F.; Theulings, A. M. M. G.; Dekker, C.; Vandersypen, L. M. K., Formation and control of wrinkles in graphene by the wedging transfer method. *Applied Physics Letters* **2012,** *101* (10), 103116; (b) Zhu, W.; Low, T.; Perebeinos, V.; Bol, A. A.; Zhu, Y.; Yan, H.; Tersoff, J.; Avouris, P., Structure and Electronic Transport in Graphene Wrinkles. *Nano Letters* **2012,** *12* (7), 3431-3436.

50.   Lu, C.-H.; Yang, H.-H.; Zhu, C.-L.; Chen, X.; Chen, G.-N., A Graphene Platform for Sensing Biomolecules. *Angewandte Chemie* **2009,** *121* (26), 4879-4881.

51.   Wong, K.-Y.; Pettitt, B. M., Orientation of DNA on a surface from simulation. *Biopolymers* **2004,** *73* (5), 570-578.

52.   Stern, E.; Wagner, R.; Sigworth, F. J.; Breaker, R.; Fahmy, T. M.; Reed, M. A., Importance of the Debye Screening Length on Nanowire Field Effect Transistor Sensors. *Nano Letters* **2007,** *7* (11), 3405-3409.

53.   Israelachvili, J. N., *Intermolecular and surface forces: revised third edition*. Academic press: 2011.

54.   Owczarzy, R.; Moreira, B. G.; You, Y.; Behlke, M. A.; Walder, J. A., Predicting Stability of DNA Duplexes in Solutions Containing Magnesium and Monovalent Cations. *Biochemistry* **2008,** *47* (19), 5336-5353.

55.   Zhang, G.-J.; Zhang, G.; Chua, J. H.; Chee, R.-E.; Wong, E. H.; Agarwal, A.; Buddharaju, K. D.; Singh, N.; Gao, Z.; Balasubramanian, N., DNA Sensing by Silicon Nanowire: Charge Layer Distance Dependence. *Nano Letters* **2008,** *8* (4), 1066-1070.

56.   Owczarzy, R.; You, Y.; Groth, C. L.; Tataurov, A. V., Stability and Mismatch Discrimination of Locked Nucleic Acid–DNA Duplexes. *Biochemistry* **2011,** *50* (43), 9352-9367.

57.   Regan, W.; Alem, N.; Alemán, B.; Geng, B.; Girit, Ç.; Maserati, L.; Wang, F.; Crommie, M.; Zettl, A., A direct transfer of layer-area graphene. *Applied Physics Letters* **2010,** *96* (11), 113102.

58.   (a) Choi, Y.-K.; Lee, J. S.; Zhu, J.; Somorjai, G. A.; Lee, L. P.; Bokor, J., Sublithographic nanofabrication technology for nanocatalysts and DNA chips. *Journal of Vacuum Science &*

Technology B **2003,** *21* (6), 2951-2955; (b) Pei, H.; Lu, N.; Wen, Y.; Song, S.; Liu, Y.; Yan, H.; Fan, C., A DNA Nanostructure-based Biomolecular Probe Carrier Platform for Electrochemical Biosensing. *Advanced Materials* **2010,** *22* (42), 4754-4758; (c) He, X.; Xu, J.; Liu, Y.; Peng, R.; Lee, S.-T.; Kang, Z., Carbon nanospheres for highly sensitive electrochemical detection of sequence-specific protein-DNA interactions. *Chemical Communications* **2011,** *47* (29), 8316-8318.

59.   (a) Hsieh, K.; Ferguson, B. S.; Eisenstein, M.; Plaxco, K. W.; Soh, H. T., Integrated Electrochemical Microsystems for Genetic Detection of Pathogens at the Point of Care. *Accounts of Chemical Research* **2015,** *48* (4), 911-920; (b) Lu, N.; Gao, A.; Dai, P.; Song, S.; Fan, C.; Wang, Y.; Li, T., CMOS-Compatible Silicon Nanowire Field-Effect Transistors for Ultrasensitive and Label-Free MicroRNAs Sensing. *Small* **2014,** *10* (10), 2022-2028.

60.   (a) Banerjee, S.; Wilson, J.; Shim, J.; Shankla, M.; Corbin, E. A.; Aksimentiev, A.; Bashir, R., Slowing DNA Transport Using Graphene–DNA Interactions. *Advanced Functional Materials* **2015,** *25* (6), 936-946; (b) Hwang, M. T.; Landon, P. B.; Lee, J.; Choi, D.; Mo, A. H.; Glinsky, G.; Lal, R., Highly specific SNP detection using 2D graphene electronics and DNA strand displacement. *Proceedings of the National Academy of Sciences* **2016,** *113* (26), 7088-7093; (c) Yang, K.; Feng, L.; Hong, H.; Cai, W.; Liu, Z., Preparation and functionalization of graphene nanocomposites for biomedical applications. *Nat. Protocols* **2013,** *8* (12), 2392-2403.

61.   (a) Glinskii, A. B.; Ma, J.; Ma, S.; Grant, D.; Lim, C.-U.; Sell, S.; Glinsky, G., Identification of intergenic trans-regulatory RNAs containing a disease-linked SNP sequence and targeting cell cycle progression/differentiation pathways in multiple common human disorders. *Cell Cycle* **2009,** *8* (23), 3925-3942; (b) Glinskii, A. B.; Ma, S.; Ma, J.; Grant, D.; Lim, C.-U.; Guest, I.; Sell, S.; Buttyan, R.; Glinsky, G. V., Networks of intergenic long-range enhancers and snpRNAs drive castration-resistant phenotype of prostate cancer and contribute to pathogenesis of multiple common human disorders. *Cell Cycle* **2011,** *10* (20), 3571-3597.

62.   Hsieh, K.; White, R. J.; Ferguson, B. S.; Plaxco, K. W.; Xiao, Y.; Soh, H. T., Polarity-Switching Electrochemical Sensor for Specific Detection of Single-Nucleotide Mismatches. *Angewandte Chemie International Edition* **2011,** *50* (47), 11176-11180.

63.   Mannoor, M. S.; Tao, H.; Clayton, J. D.; Sengupta, A.; Kaplan, D. L.; Naik, R. R.; Verma, N.; Omenetto, F. G.; McAlpine, M. C., Graphene-based wireless bacteria detection on tooth enamel. *Nature Communications* **2012,** *3*, 763.

64.   Jafari, H. M.; Abdelhalim, K.; Soleymani, L.; Sargent, E. H.; Kelley, S. O.; Genov, R., Nanostructured CMOS Wireless Ultra-Wideband Label-Free PCR-Free DNA Analysis SoC. *IEEE Journal of Solid-State Circuits* **2014,** *49* (5), 1223-1241.

65.   Yan, L.; Zheng, Y. B.; Zhao, F.; Li, S.; Gao, X.; Xu, B.; Weiss, P. S.; Zhao, Y., Chemistry and physics of a single atomic layer: strategies and challenges for functionalization of graphene and graphene-based materials. *Chemical Society Reviews* **2012,** *41* (1), 97-114.

66.   Hwang, M. T.; Landon, P. B.; Lee, J.; Mo, A.; Meckes, B.; Glinsky, G.; Lal, R., DNA nano-carrier for repeatable capture and release of biomolecules. *Nanoscale* **2015,** *7* (41), 17397-17403.

67.   Stolyarova, E.; Rim, K. T.; Ryu, S.; Maultzsch, J.; Kim, P.; Brus, L. E.; Heinz, T. F.; Hybertsen, M. S.; Flynn, G. W., High-resolution scanning tunneling microscopy imaging of mesoscopic graphene sheets on an insulating surface. *Proceedings of the National Academy of Sciences* **2007,** *104* (22), 9209-9212.

68.   Barr, M., Pulse width modulation. *Embedded Systems Programming* **2001,** *14* (10), 103-104.

69.   Briefer, D. K., Pulse width modulation digital to analog converter. Google Patents: 2001.

70.   (a) Sedra, A. S.; Smith, K. C., *Microelectronic circuits*. New York: Oxford University Press: 1998; Vol. 1; (b) Hayt, W. H.; Kemmerly, J. E.; Durbin, S. M., *Engineering circuit analysis*. McGraw-Hill New York: 1986.

71.   Box, G. E.; Jenkins, G. M.; Reinsel, G. C.; Ljung, G. M., *Time series analysis: forecasting and control*. John Wiley & Sons: 2015.